OPEN BIOLOGY

royalsocietypublishing.org/journal/rsob

Research

Cite this article: Vranas M *et al*. 2022 Selective localization of Mfn2 near PINK1 enables its preferential ubiquitination by Parkin on mitochondria. *Open Biol.* **12**: 210255.
https://doi.org/10.1098/rsob.210255

Received: 27 August 2021
Accepted: 18 November 2021

Subject Area:
biochemistry/structural biology/cellular biology/neuroscience

Keywords:
PINK1, ubiquitin, Mfn2, Parkin, mitochondria

Author for correspondence:
Jean-François Trempe
e-mail: jeanfrancois.trempe@mcgill.ca

†Both authors contributed equally to this study.

Electronic supplementary material is available online at https://doi.org/10.6084/m9.figshare.c.5752455.

THE ROYAL SOCIETY PUBLISHING

Selective localization of Mfn2 near PINK1 enables its preferential ubiquitination by Parkin on mitochondria

Marta Vranas[1,4,†], Yang Lu[1,4,†], Shafqat Rasool[1,4], Nathalie Croteau[1,4], Jonathan D. Krett[2], Véronique Sauvé[3,4], Kalle Gehring[3,4], Edward A. Fon[2], Thomas M. Durcan[2] and Jean-François Trempe[1,4]

[1]Department of Pharmacology and Therapeutics, [2]McGill Parkinson Program and Neurodegenerative Diseases Group, Montreal Neurological Institute and Department of Neurology and Neurosurgery, [3]Department of Biochemistry, and [4]Centre de Recherche en Biologie Structurale, McGill University, Montréal, Québec, Canada

MV, 0000-0002-4296-9018; SR, 0000-0002-5223-8358; JDK, 0000-0003-4964-3341; VS, 0000-0002-5981-4573; KG, 0000-0001-6500-1184; EAF, 0000-0002-5520-6239; TMD, 0000-0003-3942-1956; J-FT, 0000-0002-6543-3371

Mutations in Parkin and PINK1 cause early-onset familial Parkinson's disease. Parkin is a RING-In-Between-RING E3 ligase that transfers ubiquitin from an E2 enzyme to a substrate in two steps: (i) thioester intermediate formation on Parkin and (ii) acyl transfer to a substrate lysine. The process is triggered by PINK1, which phosphorylates ubiquitin on damaged mitochondria, which in turn recruits and activates Parkin. This leads to the ubiquitination of outer mitochondrial membrane proteins and clearance of the organelle. While the targets of Parkin on mitochondria are known, the factors determining substrate selectivity remain unclear. To investigate this, we examined how Parkin catalyses ubiquitin transfer to substrates. We found that His433 in the RING2 domain contributes to the catalysis of acyl transfer. In cells, the mutation of His433 impairs mitophagy. In vitro ubiquitination assays with isolated mitochondria show that Mfn2 is a kinetically preferred substrate. Using proximity-ligation assays, we show that Mfn2 specifically co-localizes with PINK1 and phospho-ubiquitin (pUb) in U2OS cells upon mitochondrial depolarization. We propose a model whereby ubiquitination of Mfn2 is efficient by virtue of its localization near PINK1, which leads to the recruitment and activation of Parkin via pUb at these sites.

1. Introduction

Mutations in the *PRKN* gene cause autosomal recessive Parkinson's disease (PD) [1]. The Parkin protein is a RING1-In-Between-RING2 (RBR) E3 ubiquitin ligase implicated in many cellular processes, including mitochondrial quality control, innate immunity and cellular survival pathways [2]. Activation of Parkin on mitochondria requires PINK1, a kinase whose mutations also cause autosomal recessive PD [3]. PINK1 selectively builds up on damaged mitochondria through an elaborate import and proteolysis pathway. In normal polarized mitochondria, PINK1 is imported via its mitochondrial-targeting sequence (MTS) and cleaved by the mitochondrial-processing peptidase and PARL protease [4,5]. PINK1 is then ubiquitinated and degraded in the cytosol [6,7]. This turnover results in a low level of PINK1 on healthy mitochondria. However, when mitochondria are depolarized, such as with the protonophore carbonyl cyanide m-chlorophenyl hydrazone (CCCP), the MTS of PINK1 is no longer processed and forms a 750 kDa complex with the translocase of the outer membrane (TOM), which leads to its accumulation [8–11]. PINK1 then

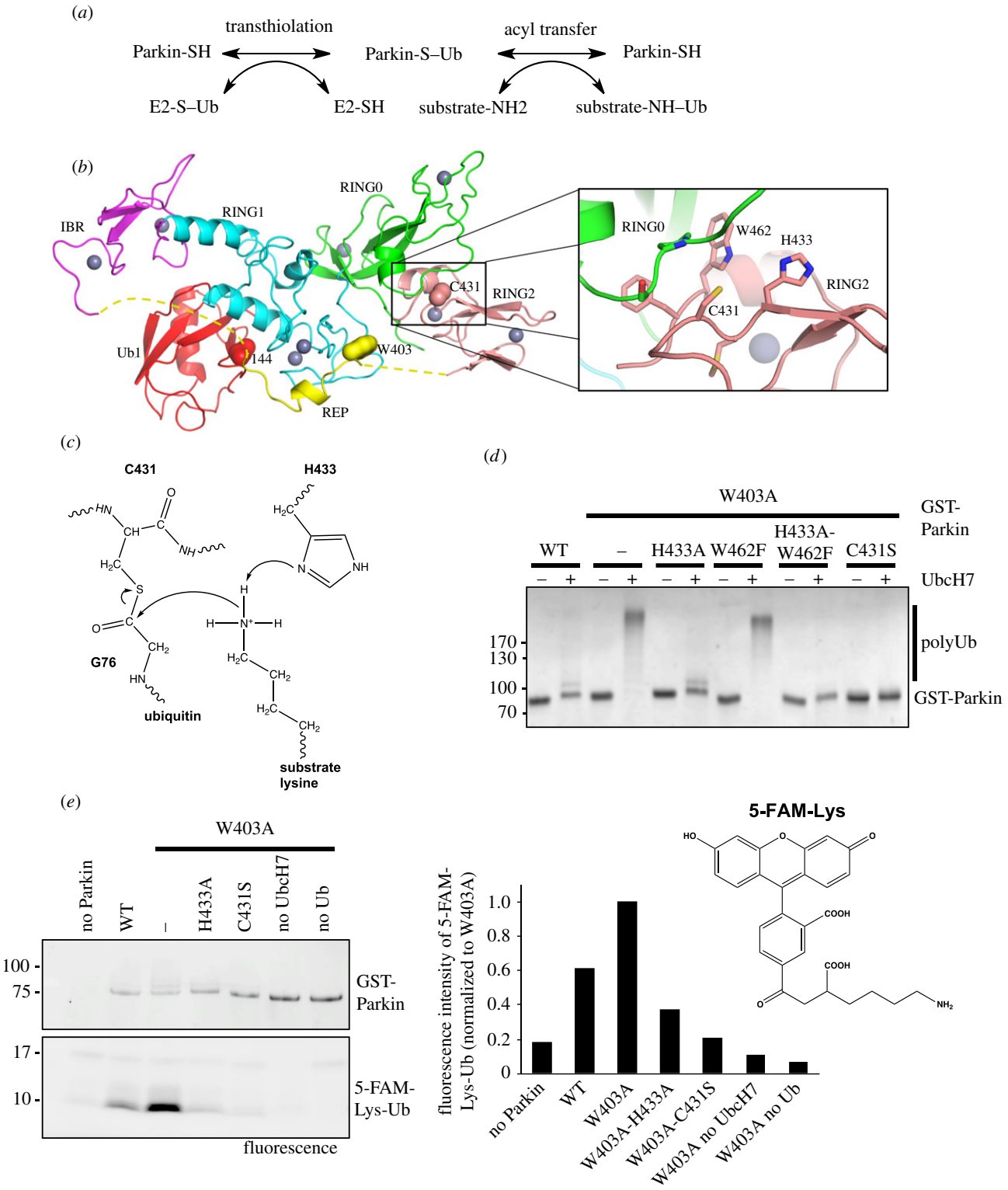

Figure 1. Parkin His433 contributes to the catalysis of Ub transfer. (*a*) Two-step reaction mechanism for substrate ubiquitination by Parkin. (*b*) Left: crystal structure of apo rat Parkin (PDB 4ZYN) showing the different domains of Parkin and the position of residues Trp403 and Cys431. Right: RING0 and RING2 interface with highlighted active site residues Cys431, His433 and Trp462. (*c*) CBB-stained SDS-PAGE of autoubiquitination assay products for GST-Parkin with different active site mutations. (*d*) Ubiquitination reactions with GST-Parkin mutants and fluorescein Lys (5-FAM-Lys). Products were resolved by SDS-PAGE and visualized by fluorescence. Quantification of the 5-FAM-Lys-Ubiquitin adduct is shown normalized to W403A. (*e*) Model for the catalysis of isopeptide bond formation by Parkin: His433 retrieves a proton from the side-chain amino group of a lysine, which performs a nucleophilic attack on the Cys431–Ub thioester bond.

autophosphorylates in *trans* at Ser228, which enables its kinase domain to bind and phosphorylate ubiquitin on Ser65 [12–14]. Phospho-ubiquitin (pUb) in turn recruits and activates Parkin by phosphorylation [9–11,15–18]. Phospho-Parkin then ubiquitinates proteins on the outer mitochondrial membrane (OMM) [19–21]. This induces either the recruitment of autophagy receptors for the initiation of mitophagy, or the formation of mitochondria-derived vesicles (MDVs) [22–24].

RBR E3 ligases like Parkin function through a two-step mechanism to transfer ubiquitin to a substrate, similar to that employed by HECT-type ligases (figure 1*a*). The

RING1 domain binds to an E2 enzyme charged with ubiquitin via a thioester bond and transfers ubiquitin to an acceptor cysteine in the RING2 catalytic domain to form a thioester intermediate. Ubiquitin is then transferred to an amino group via an acyl transfer reaction to form a stable isopeptide bond. This discovery stemmed from the observation that the E2 enzyme UbcH7, also known as UBE2L3, can only transfer ubiquitin via transthiolation, which limits its action to RBR or HECT ligases that have an acceptor cysteine [25]. UbcH7 is part of a subset of E2 enzymes that bind to Parkin and mediate PINK1-depending mitophagy [26]. As most PD mutations in Parkin either abrogate protein translation or inactivate its biochemical activity (e.g. mutation of the acceptor C431F in the RING2 domain), its biochemical activity is neuroprotective. It is thus crucial to understand how this E3 ligase is activated by PINK1 and to elucidate the mechanism by which it transfers ubiquitin to a substrate.

The crystal structure of full-length Parkin in its *apo*, non-phosphorylated form, revealed a network of auto-inhibitory interactions that explains why the ligase is inactive in the basal state (figure 1*b*) [27–29]. Parkin contains four zinc finger domains named RING0, RING1, IBR and RING2, of which only RING1 adopts the cross-brace topology characteristics of RING domains that bind E2 ubiquitin-conjugating enzymes. The repressor element of Parkin (REP) binds RING1 and blocks its E2-binding site. The REP is anchored to RING1 via Trp403, and indeed mutation of this residue leads to hyperactivation of Parkin [27]. The ubiquitin-like (Ubl) domain also binds to a site in RING1 adjacent to the E2-binding site [27], in agreement with a previous report showing that the Ubl also inhibits Parkin's ligase activity [30]. In addition, the RING0 domain occludes the ubiquitin acceptor site Cys431 in RING2, thus further reducing its activity. Following PINK1 activation, pUb binds to Parkin RING1-IBR domains, which induces the dissociation of the Ubl domain [31–34] and its subsequent phosphorylation by PINK1 on Ser65 [12,35]. The structure of insect phospho-Parkin in complex with pUb and UbcH7 [36] and the structure of human phospho-Parkin bound to pUb [37] were solved by X-ray crystallography. Both structures revealed that the phosphorylated Ubl domain binds to the RING0 domain, which induces the dissociation of the REP and RING2 domains, and E2 binding on RING1 [36,37]. The catalytic RING2 is thus free and can bind to the E2–Ub conjugate complex to allow the transfer of ubiquitin onto Cys431 linked by a thioester bond. Obstruction of the E2-binding site by the REP and occlusion of the active site Cys431 by RING0, as well as the inability to observe the formation on an oxyester-linked Ub on the Parkin RBR C431S mutant [25], suggests that transthiolation is the rate-limiting step in Parkin.

While structural and biochemical work provided much insight into the conformational changes that enable thioester transfer from an E2 enzyme to Parkin, the subsequent transfer of ubiquitin to a substrate remains far less understood. The formation of an isopeptide bond by HECT or RBR ligases involves the transfer of the ubiquitin carboxy terminus from a cysteine thiol on the ligase to a substrate amino group, typically the side-chain of a lysine [38,39]. However, the pKa of these amino groups is typically between 9.5 and 11.5, and they are thus mostly protonated at near-neutral physiological pH [40]. For the nucleophilic attack reaction to proceed, the primary amino group needs to be deprotonated. The crystal structures of *apo* Parkin [27–29] and the solution NMR structure of the RING2 domain from fly Parkin [41] revealed that human His433, a residue conserved in other RBR ligases, could act as a general base to catalyse acyl transfer. His433 is adjacent to Cys431, and NMR analysis showed that this histidine is deprotonated at neutral pH and could serve as a proton acceptor [41]. The mutation H433A indeed reduced autoubiquitination activity of apo Parkin [27–29,41]. Mutation of the corresponding histidine in the RBR protein HOIP (His887) traps the HOIP–Ub thioester conjugate, which is consistent with a general base role for this histidine [42]. However, this has not been demonstrated for Parkin, and the pH dependence of Parkin H433A and H433N mutants' reactivity with ubiquitin vinyl sulfone suggests that it also modulates the pKa of the thiol group on Cys431, which could affect thioester transfer [29].

By contrast with HOIP, which selectively synthesizes linear polyubiquitin chains, Parkin is less selective and can conjugate all lysine side-chains on ubiquitin, primarily Lys6, Lys11, Lys48 and Lys63 [43,44]. It can also conjugate ubiquitin to lysine side-chains on itself as well as vast array of intracellular proteins, mostly proteins located at the OMM following mitochondrial depolarization [19,20,43,44]. While this would seem to indicate that Parkin does not display any specificity, recent studies suggest otherwise. Quantitative proteomics and dynamic analysis in HeLa cells and neurons with low (endogenous) levels of Parkin show that different sites on OMM proteins build up at different rates in the first hour following depolarization with oligomycin/antimycin A (OA) [45]. The most abundant ubiquitinated sites are found in voltage-dependent anion channel (VDAC)1-3, the most abundant OMM proteins, followed by Mfn2, CISD1, RHOT1, FAF2, HK1, TOMM20 and TOMM70. In another study from our own group, we found that Mfn1 and Mfn2 were ubiquitinated and degraded more rapidly than the other substrates following addition of CCCP [46]. Others had also previously observed that Mfn1/Mfn2 are extensively ubiquitinated by Parkin [20,21,47]. Mfn1/Mfn2 (Mitofusins) are membrane-anchored GTPases that mediate the fusion of the OMM and play a critical role in regulating fusion/fission cycles and mitochondrial quality control [48]. While Mitofusins are not essential for Parkin recruitment [18], a subsequent study found that Mfn2 can recruit Parkin in a PINK1-dependent manner, and Mfn2-deficient mice have impaired mitophagy in the heart [49].

Here, we exploit recent structural and proteomics findings to understand the biochemical basis for substrate ubiquitination by Parkin. We find that His433 acts as a base that accelerates the acyl transfer step, but is minimally involved in thioester transfer from the E2–Ub complex. Mutation of His433 had a mild effect on mitochondrial Parkin recruitment, but a stronger effect in mitophagy. Ubiquitination assays with isolated mitochondria showed that at low Parkin concentration, Mfn2 is efficiently ubiquitinated, whereas other OMM proteins are not. In this assay, mutation of His433 only mildly affects Mfn2 ubiquitination, which is consistent with a model where Mfn2 is optimally positioned to receive ubiquitin from Parkin following activation, and thus for which the acyl transfer step is not the rate-limiting step. Using proximity-ligation assays (PLAs), we demonstrate that PINK1 localizes in proximity to Mfn2, but not with other substrates, which explains why Parkin rapidly ubiquitinates Mfn2.

2. Results

2.1. Parkin His433 contributes to the catalysis of Ub transfer to a Lys ε amino group

The structure of the RING2 domain shows that the active site Cys431 is surrounded by two side-chains with acid/base chemical groups that could affect the pKa of an incoming substrate amino group: His433 and Trp462 (figure 1*b*). To test the role played by these two residues on acyl transfer catalysis, we mutated them to Ala and Phe, respectively, and performed *in vitro* autoubiquitination assays where we monitored the formation of polyubiquitin chains on Parkin after incubation with E1, UbcH7, Ub and ATP-Mg. Because apo wild-type (WT) Parkin is essentially inactive, we performed these experiments in the context of the W403A mutant of Parkin, which releases auto-inhibition [27]. The results confirm that the W403A mutant autoubiquitinates to a greater extent than WT Parkin (figure 1*c*). When paired with a mutation on the active site that inactivates ligase activity, C431S, the double mutant W403A-C431S displays almost no activity. Crucially, the double mutant W403A-H433A has impaired ubiquitination, whereas the W462F mutation has no effect on activity. The triple mutant W403A-H433A-W462F shows less activity than the W403A-H433A mutant. This suggests that His433 plays a major role in ubiquitination, whereas Trp462 plays a minor role.

To investigate the acyl transfer of ubiquitin from Parkin to a substrate Lys ε amino group, a fluorescence lysine compound (5-FAM-Lys; figure 1*d*) was added to the ubiquitination reaction mix. After 2 h incubation, SDS-PAGE-resolved products were quantified by fluorescence at 488 nm (figure 1*d*). A control N-terminal 5-FAM-labelled ubiquitin and reactions lacking either UbcH7 or Ub were included. The results show that 5-FAM-Lys-Ub formation is observed in WT Parkin and is enhanced by the W403A mutation. In the W403A background, the two active site mutants C431S and H433A show reduced 5-FAM-Lys-Ub formation. Based on the three-dimensional structure of Parkin [27] and these *in vitro* biochemical assays, we propose a model for the catalysis of isopeptide bond formation by Parkin whereby His433 retrieves a proton from the side-chain amino group of a lysine, which performs a nucleophilic attack on the Cys431–Ub thioester bond (figure 1*e*).

2.2. Parkin His433 is not essential for transthiolation

The reduced activity of the H433A mutant could also result from an impairment in thioester transfer of Ub from the E2 to Parkin Cys431. In order to assess transthiolation directly, single-turnover assays were performed. We used ubiquitin-loaded E2 (UbcH7–Ub) and monitored disappearance of UbcH7–Ub and autoubiquitination of Parkin through time. The products were resolved by SDS-PAGE and confirm that the hyperactive W403A mutant discharges UbcH7–Ub faster than WT (compare 2 min and 5 min time points), whereas mutation of Cys431 abolishes discharging (figure 2*a*; electronic supplementary material, figure S1a). The W403A-H433A mutant discharges at the same rate as W403A, but fails to autoubiquitinate, which is consistent with His433 being required for acyl transfer and not transthiolation. The structure of auto-inhibited Parkin also shows that the side-chain of Glu444 forms a polar interaction with His433 and thus could affect acyl transfer catalysis. We thus tested the mutation E444Q, a naturally occurring variant that does not impair mitophagy and has uncertain clinical significance for PD [50]. The double mutant W403A-E444Q discharges UbcH7–Ub similarly to W403A, but can still form polyubiquitin chains, suggesting it does not play a major role in either reaction.

One prediction from our model is that the H433A mutant would still be able to form a thioester Parkin–Ub complex. To detect thioester formation in Parkin, we used fluorescently labelled ubiquitin (fluorescein-Ub, FluoUb) to monitor ubiquitinated species on Parkin. Reactions were stopped in the presence of either tris(2-carboxyethyl)phosphine (TCEP), which breaks only disulfide bonds, or dithiothreitol (DTT), which reduces both disulfide and thioester bonds. Ub linkages were observed by SDS-PAGE analysis and fluorescence imaging. The results show that UbcH7–Ub is completely discharged by the DTT treatment, as expected. The gel also shows a mono-ubiquitinated form of Parkin W403A-H433A that is visible with TCEP and reduced by 60% upon addition of DTT, consistent with a mixture of isopeptide and thioester formation (figure 2*b*; electronic supplementary material, figure S1b). By contrast, small differences are observed in Parkin-Ub levels between TCEP and DTT for WT and W403A, showing that these bands are not thioester-linked.

We next decided to investigate discharging of UbcH7–Ub in the context of Parkin activation by phosphorylation. Parkin was phosphorylated *in vitro* by PINK1 as described previously [35]. Discharging reaction mixes were prepared with different concentrations of inactive or activated Parkin. Here, His433 was mutated to a Phe, which has a bulky side-chain similar to His, but lacking acid/base chemical groups. Inactive, dephosphorylated Parkin does not significantly discharge UbcH7–Ub, in both WT and H433F backgrounds. Once phosphorylated, both WT and H433F Parkin show increased UbcH7–Ub discharging (figure 2*c*). Altogether, the data are consistent with His433 being involved in acyl transfer of ubiquitin to a substrate lysine, but not in thioester transfer.

2.3. Mutation of Parkin His433 affects mitophagy

Upon mitochondrial damage, PINK1-dependent Parkin activation and translocation from the cytosol to the mitochondria leads to the build up of Ub chains and triggers mitophagy [9–11,18]. We thus sought to investigate the impact of ubiquitin acyl transfer impairment on Parkin recruitment and mitophagy. We used U2OS cells stably expressing green fluorescent protein (GFP)-Parkin WT, H433F or C431S. Cells were treated with CCCP to induce mitochondria membrane depolarization and imaged to track GFP-Parkin recruitment to Tom20-labelled mitochondria. As previously observed, the C431S mutant was completely impaired in recruitment (figure 3*a*). By contrast, the H433F mutant was recruited to mitochondria, albeit more slowly than WT (figure 3*a*). We indeed observe that the H433F mutant is capable of ubiquitinating OMM substrates such as Mfn1/2 and VDAC in cells (figure 3*b*), in line with the proposed positive feedback mechanism boosting Parkin recruitment, but in apparent contradiction of our *in vitro* results. However, when we quantified cells negative for Tom20-mitochondria after 24 h of CCCP treatment (mitophagy), cells expressing the mutants H433F and C431A were

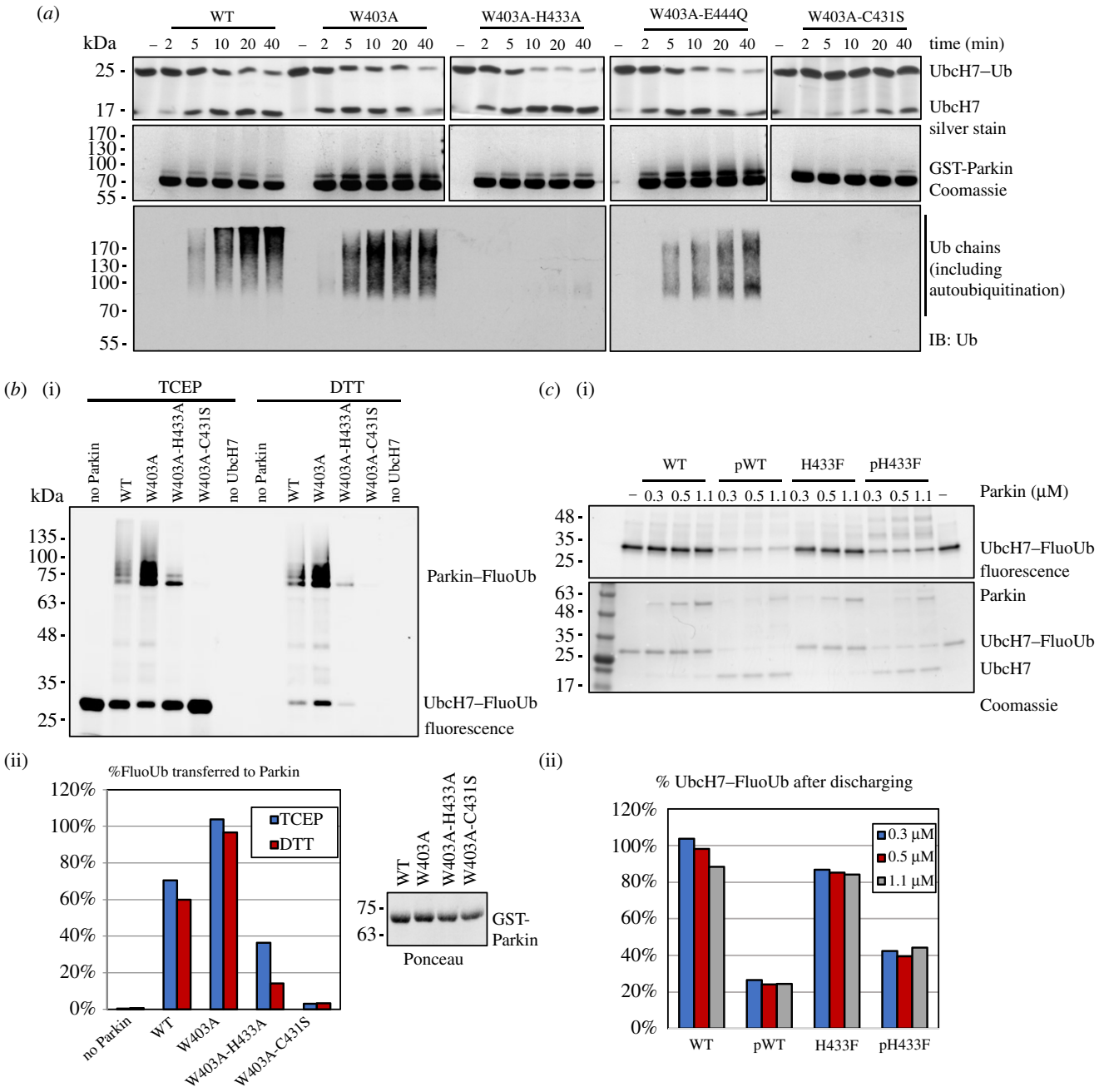

Figure 2. Parkin His433 is not essential for transthiolation. (*a*) Immunoblots (top) and CBB-stained SDS-PAGE (bottom) of UbcH7–Ub discharge assays with GST-Parkin WT and mutants. Reactions were stopped with sample buffer containing TCEP to reduce disulfide bonds but keep thioester bonds intact. (*b*) (i) SDS-PAGE fluorescent scan showing Ub-linkage after mixing fluorescein-labelled Ub (FluoUb), E1, ATP and UbcH7 with GST-Parkin and stopping the reaction with TCEP or DTT. (ii) Quantification of FluoUb transferred to Parkin as a percentage of UbcH7–FluoUb in the absence of Parkin. Loading controls for GST-Parkin proteins are shown at the bottom right. (*c*) (i) Fluorescent scan and Coomassie-stained SDS-PAGE showing UbcH7–FluoUb discharging by increasing concentrations of Parkin or phosphorylated Parkin. (ii) Quantification of Ub loaded UbcH7 (UbcH7–FluoUb) after reaction.

both significantly impaired in comparison with WT (figure 3*c*; electronic supplementary material, figure S2). Furthermore, the distribution of diffuse and puncta GFP-Parkin in cells after 24 h of CCCP treatment was also altered by the H433F mutation (figure 3*d*; electronic supplementary material, figure S2). These data directly associate challenges in ubiquitin acyl transfer with impaired mitophagy.

2.4. Ubiquitination assays on isolated mitochondria reveal preference for Mfn2

In order to understand how substrate ubiquitination might be differentially affected by mutation of His433 in cells, we set up a series of *in organello* ubiquitination assays, a cell-free assay with isolated mitochondria previously described [35]. Briefly, HeLa cells, which lack Parkin, can be treated with CCCP to allow PINK1 build up at the OMM prior to the isolation of mitochondria. The addition of a ubiquitination mix (ATP, E1, UbcH7 and Ub) and recombinant catalytically active Parkin to isolated mitochondria is sufficient to ubiquitinate OMM substrate Mfn2 (figure 4*a*).

Reaction products were resolved by SDS-PAGE and positive ubiquitination observed by the formation of high molecular weight bands and loss of the unmodified band. Results show that extensive ubiquitination of Mfn2 is dependent on both depolarization of mitochondria and the presence of the Parkin (figure 4*a*). Ubiquitination of Mfn2

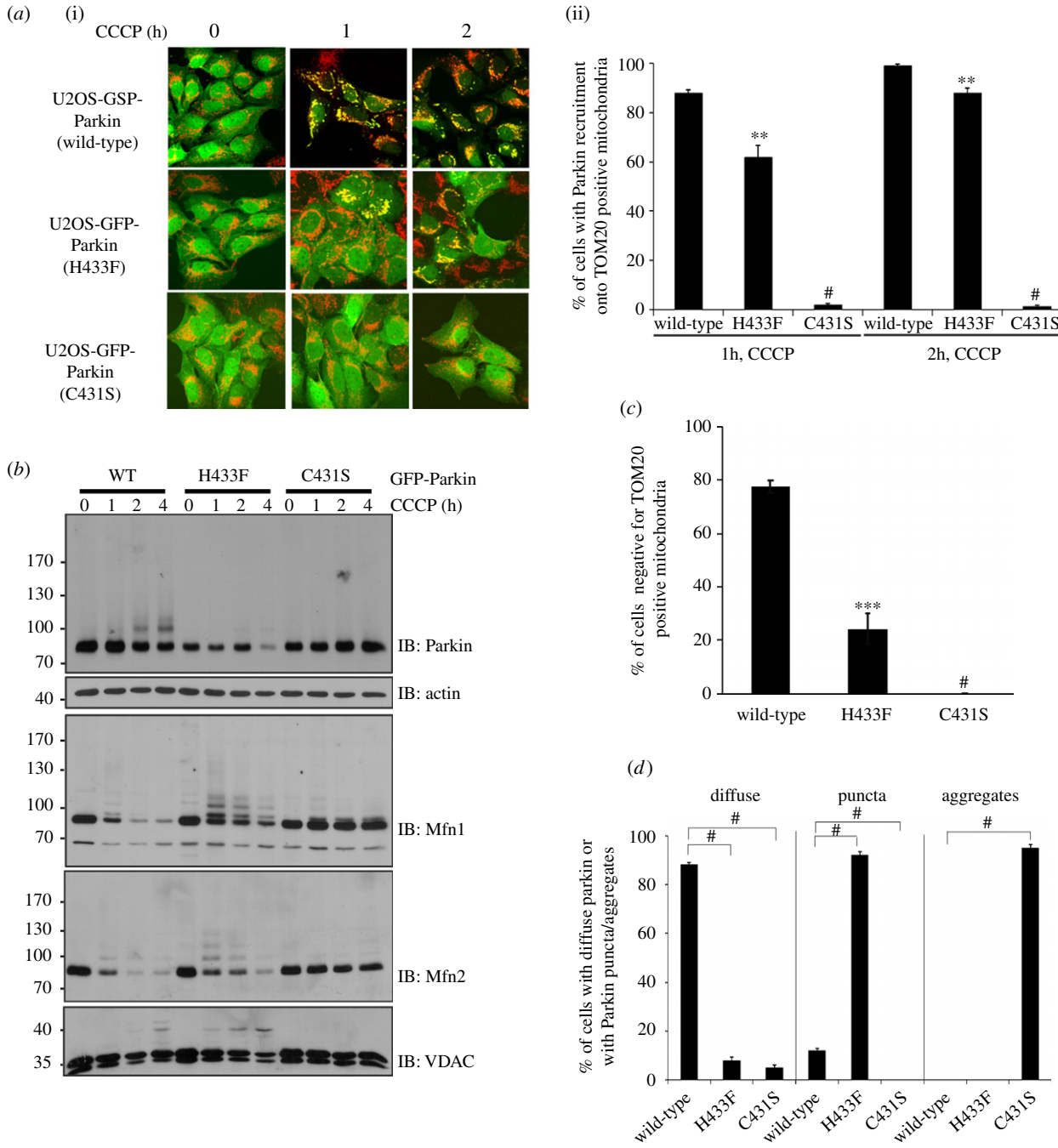

Figure 3. His433 is required for efficient Parkin mitochondrial recruitment. (*a*) Confocal microscopy images showing (i) recruitment of stably expressed GFP-Parkin WT, H433F or C431S to mitochondria (Tom20 antibody in red) in U2OS cells and (ii) quantification of the percentage of GFP- Parkin on mitochondria ($n = 3$, two-way ANOVA, with Tukey post-test). (*b*) Western blot showing ubiquitination of mitochondrial proteins in U2OS cells after CCCP treatment. (*c*) Quantification of Tom20-negative U2OS cells expressing recombinant Parkin after 24 h of CCCP treatment from immunofluorescence microscopy (100 cells analysed per condition in three independent blinded experiments, two-way ANOVA, with Bonferroni post-test). (*d*) Dispersion of GFP-Parkin in cells after 24 h of CCCP treatment ($n = 3$, two-way ANOVA, with Tukey post-test). #$p < 0.0001$; ***$p < 0.001$; **$p < 0.01$.

under these conditions is insensitive to the active site H433A mutation and proportional to the amount of Parkin in the reaction (figure 4*b*; electronic supplementary material, figure S3a). While monoubiquitination of VDAC can be observed at high concentrations of Parkin, there is little loss of the unmodified band compared to Mfn2. This difference in the extent of ubiquitination between VDAC and Mfn2 suggests a kinetic advantage for Mfn2.

The amino group of lysine side-chains is typically protonated at neutral pH, and they are intrinsically poor nucleophiles. Given the proposed role of His433 to act as a base to deprotonate any substrates' lysine side-chain in order to facilitate the acyl transfer step, *in organello* ubiquitination assays were performed to assess the effects of deprotonation. The time course of ubiquitination at two different pHs (7.0 and 7.4) shows no difference between WT and H433A Parkin in Mfn2 ubiquitination. When we tested a wider pH range, Mfn2 ubiquitination still presented the same pattern for both WT and H433F variants (electronic supplementary material, figure S3b). Yet, the overall ubiquitination levels detected at high molecular weight protein bands was significantly affected when His433 was mutated. Since we have shown that mutation of His433 reduces acyl transfer but not thioester transfer, these *in organello* data imply that the rate-limiting step for Mfn2 ubiquitination is thioester transfer. However, acyl transfer is the rate-limiting step for

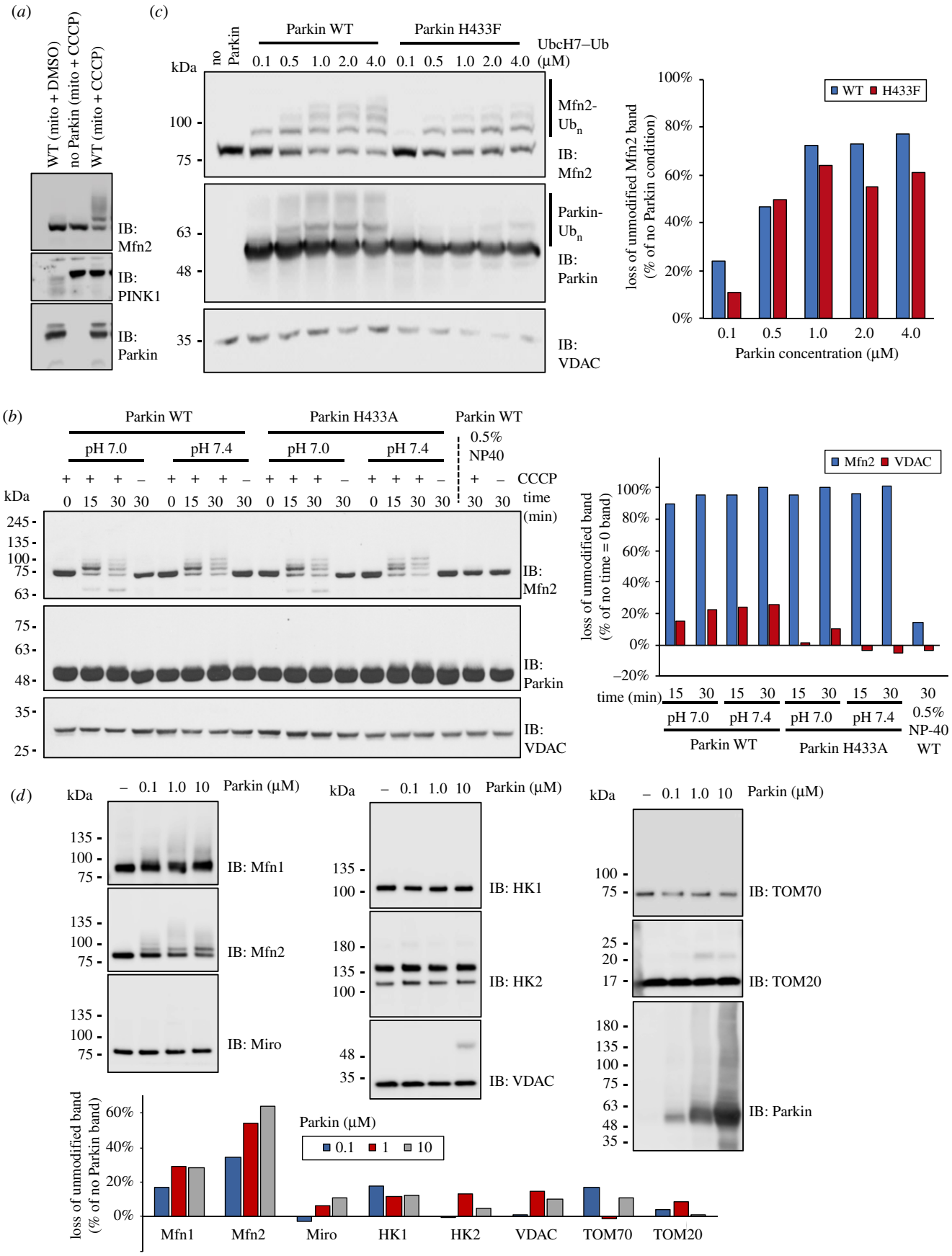

Figure 4. Ubiquitination assays on isolated mitochondria reveal preference for Mfn2. (*a*) *In organello* ubiquitination assay. Mitochondria isolated from HeLa cells, treated or not with CCCP are added to a ubiquitination mix (ATP, E1, UbcH7 and Ub) and recombinant Parkin. Ubiquitinated products are detected by western blot analysis. (*b*) Immunoblot of *in organello* ubiquitination assay testing activity of active site H433A mutation at different pH and time. Quantification of unmodified VDAC and Mfn2 bands is shown on the right. (*c*) Immunoblot of *in organello* ubiquitination assay testing activity of active site H433F mutation at different concentrations of Ub-loaded UbcH7 (UbcH7–Ub). Quantification of unmodified band is shown on the right. (*d*) Immunoblots of *in organello* ubiquitination assays to evaluate ubiquitination levels of OMM proteins. Quantification of unmodified bands is shown below.

autoubiquitination *in vitro* (figures 1 and 2), and overall ubiquitination of mitochondrial proteins (electronic supplementary material, figure S3b). Indeed, if we use pre-charged Ubch7–Ub *in organello*, we observe a small reduction in Mfn2 ubiquitination by the H433F mutant (figure 4*c*). Since thioester transfer is independent of the substrate, these data are pointing to Mfn2 being a kinetically preferred substrate for acyl transfer.

We next sought to evaluate ubiquitination of known OMM proteins by Parkin in *in organello* assays using recombinant WT Parkin in a concentration range from 0 to 10 µM. Products were resolved by SDS-PAGE and immunoblotted for the different proteins. Results confirm that Mfn2 is readily ubiquitinated for concentrations of Parkin as low as 0.1 µM (figure 4*d*). Mfn1 is also ubiquitinated in a similar fashion, though its ubiquitination pattern is less prominent than Mfn2. The remaining substrates are not substantially ubiquitinated and mostly remain unmodified even at the highest Parkin concentration (figure 4*d*). This confirms that Mfn2 is a kinetically preferred substrate.

Binding of Parkin to pUb and Parkin phosphorylation by PINK1 are necessary for Mfn2 ubiquitination *in organello* [35]. Parkin phosphorylation releases the RING2 domain and allows it to interact with substrates [36]. Given that Mfn2 is conjugated to pUb in cells [46], this suggests that Parkin's substrate selectivity may be largely dictated by the proximity of PINK1 to Mfn2 on mitochondrial membranes. In support of this model, we found that addition of the non-denaturing detergent NP40, which solubilizes mitochondrial membranes into micelles, abrogates Mfn2 ubiquitination *in organello* even in the presence of CCCP (figure 4*b*; last two lanes). However, similar detergent concentrations did not affect Parkin's E3 ubiquitin ligase activity *in vitro* (electronic supplementary material, figure S3c). Thus, membrane integrity is critical for Mfn2 ubiquitination by Parkin. This suggests that a critical step for substrate selectivity is pUb labelling of substrates that are in proximity to PINK1 on the OMM, which would recruit Parkin at those sites and enable its phosphorylation and activation.

2.5. Parkin ubiquitinates substrates conjugated to phospho-ubiquitin

To explore the model by which pUb labelling and Parkin phosphorylation drive substrate selectivity, we set up *in vitro* ubiquitination assays where we used purified glutathione-S-transferase (GST) as 'bait' fused to either ubiquitin (GST-Ub) or phosphorylated-Ub^{Ser65} (GST-pUb^{S65}). In a series of reactions, purified Parkin or phospho-Parkin (100 nM) was incubated with a sole donor Ub source, UbcH7–Ub (4 µM), in addition to GST-Ub or GST-pUb^{S65} (2 µM) as substrates (figure 5*a*). In the absence of the E1 ubiquitin-activating enzyme, the GST-Ub substrates cannot be used as a donor Ub. Reactions were resolved by SDS-PAGE and products analysed by immunoblotting. When UbcH7–Ub was mixed with non-phosphorylated Parkin alone or in the presence of GST-Ub, little ubiquitination was observed (figure 5*b*; lanes 5, 7). When UbcH7–Ub was mixed with phosphorylated Parkin instead, alone or in the presence of GST-Ub, autoubiquitination levels increased (figure 5*b*; lane 6, 11) as expected, but no substantial GST-Ub ubiquitination was observed. When GST-pUb^{S65} is used instead, Parkin autoubiquitination is increased and, critically, GST-pUb^{S65} ubiquitination is detected, as observed in the appearance of a ladder in pUb and Ub blots (figure 5*b*, lane 8). Most strikingly, ubiquitination of GST-pUb^{S65} was further increased in the presence of phospho-Parkin, as observed in the Ub and pUb blots as well as loss of the unmodified GST-pUb band in the Ponceau stain (figure 5*b*, lane 12).

To confirm and determine where GST-pUb^{S65} was ubiquitinated, and also because ubiquitination of GST probably affects the immunoreactivity of the anti-GST antibody, we analysed the reaction products with trypsin digestion and mass spectrometry (figure 5*c*; electronic supplementary material, figure S4a). Products from reactions containing UbcH7/UbcH7-Ub, Phospho-Parkin and either GST-Ub (figure 5*b*; lanes 9, 11) or GST-pUb^{S65} (figure 5*b*; lanes 10, 12) were analysed using MaxQuant to identify and quantify lysine residues modified with the Gly-Gly motif left after trypsin cleavage of the Ub C-terminus. Two solvent-exposed lysine residues in GST (Lys45 and Lys131) were strongly ubiquitinated in GST-pUb^{S65} and could not be detected in GST-Ub (figure 5*c*; electronic supplementary material, figure S4b). Weaker sites were identified elsewhere and showed a similar pattern (electronic supplementary material, figure S4a). Because of its low abundance in the reaction mix, Parkin peptides were difficult to detect, but ubiquitination sites were identified on two lysine residues located in the Ubl-RING0 linker. Intriguingly, we observed differences in the distribution of Ub linkage types (Lys11, Lys48 and Lys63) between GST-Ub and GST-pUb^{S65}, with a massive increase in Lys48 linkage detected in the GST-pUb^{S65} sample (figure 5*c*; electronic supplementary material, figure S3b). This may reflect changes in the distributivity of donor Ub, which form shorter and more widely distributed chains in the presence of GST-pUb^{S65} (figure 5*b*, lane 12), and longer chains in its absence, predominantly on Parkin (figure 5*b*, lane 11). Together, these data support the hypothesis that when a protein is phospho-ubiquitinated, it is predisposed to be a preferential substrate for ubiquitination by phospho-Parkin.

2.6. PINK1 co-localizes with Mfn2 on damaged mitochondria

Given our previous observations about the role of pUb in dictating substrate selectivity, and the extensive Mfn2 ubiquitination observed in cells and *in organello*, we hypothesize that Mfn2 localizes near PINK1, thus making Mfn2-Ub conjugates more likely to be phosphorylated. To test this idea, PLAs were performed in U2OS cell lines [51]. PLA is an antibody-based assay that detects contact sites between proteins within approximately 40 nm by producing fluorescent signals at the sites of interaction, which can then be visualized with confocal microscopy (figure 6*a*).

Because of technical challenges in labelling both endogenous PINK1 and Mfn2 with antibodies from different species, as required for PLA, a CMV(d1) promoter-driven PINK1-HA plasmid was used [52]. PINK1 expressed from this plasmid accumulates on depolarized mitochondria and generates pUb chains [12]. Experiments were performed in both WT and PINK1 knockout (KO) cells, as well as Mfn2 KO cells as negative controls (figure 6*b*). Results show that PINK1

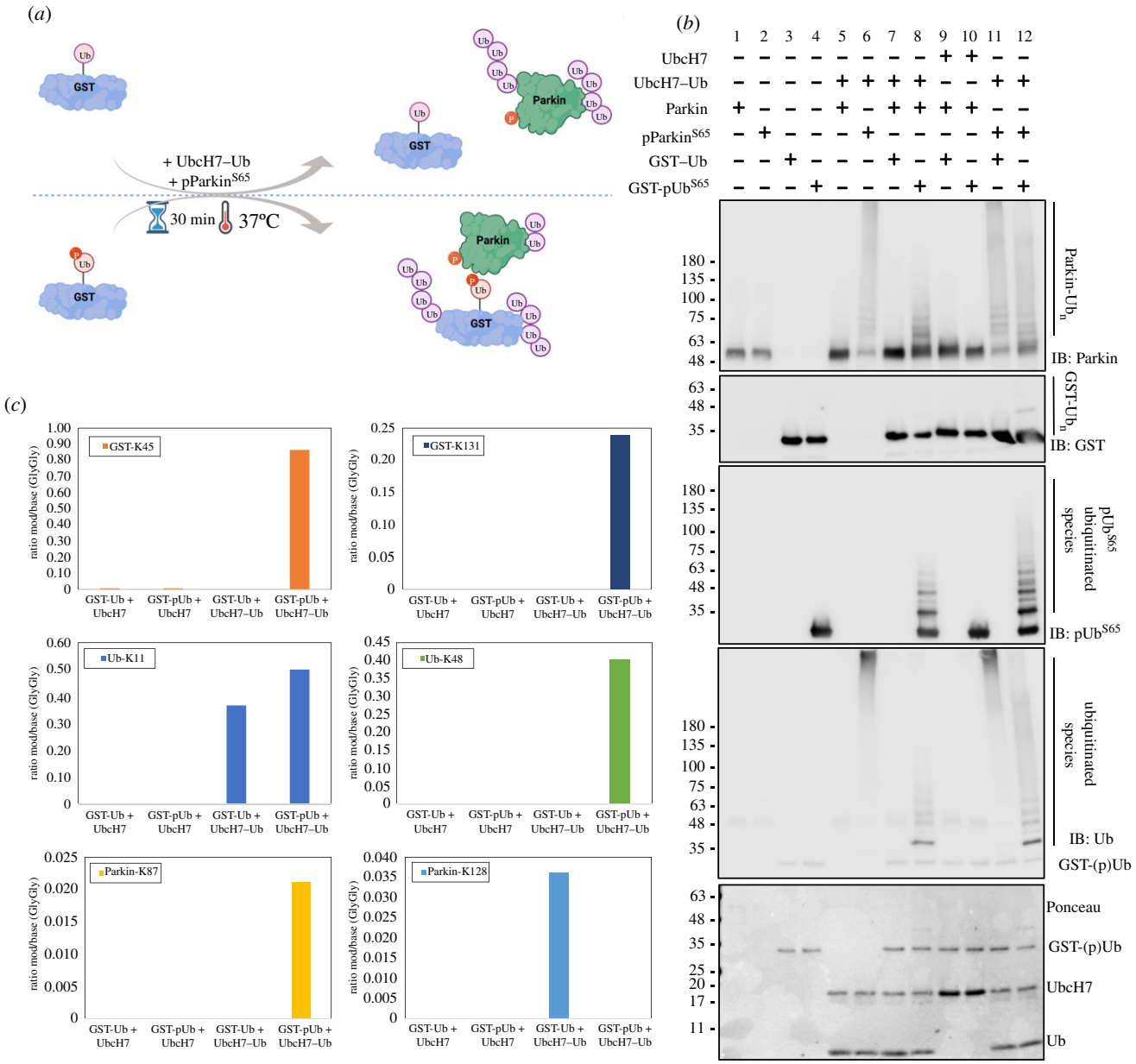

Figure 5. Parkin preferably ubiquitinates substrates tethered to phospho-ubiquitin. (*a*) Schematics of the ubiquitination assay where GST fused to either ubiquitin (GST-Ub) or phosphorylated ubiquitin (GST-pUb^{S65}) was used as a Ub acceptor and shown in (*b*). (*b*) Immunoblots of the ubiquitination assay where purified Parkin or phosphorylated Parkin (pParkin^{S65}) was incubated with UbcH7–Ub as an ubiquitin source and GST-Ub or GST-pUb^{S65} as the ubiquitin acceptor. Lanes 1 to 10 are reaction controls. Bands at around 48 kDa in lanes 1, 2, 5, 7, 9 and 10 are cross reactive bands. (c) Mass spectrometry analysis of the ubiquitination sites found for lanes 9 to 12 shown in (*b*). Selected sites in GST, Ub and Parkin molecules are shown.

(endogenous or ectopic) accumulates in the presence of CCCP, independently of Mfn2.

PLA experiments targeting Mfn2 and PINK1-HA (anti-HA) were first performed and the fluorescent spots corresponding to close contact sites between the two labelled proteins quantified. To define the region of interest (ROI) for quantification, we have labelled the endoplasmic reticulum (ER) with an anti-calnexin antibody compatible with PLA, because Mfn2 localizes at ER-mitochondrial contact sites [53] and also because the strong staining facilitated automatic ROI identification for every cell (electronic supplementary material, figure S5). Results show that an average of less than 5 PLA spots per cell were counted in negative controls where either PINK1 or Mfn2 is absent (figure 6*c*,*d*; electronic supplementary material, figure S6a). Few PLA spots are also observed in cells without CCCP treatment, where there is no mitochondrial depolarization causing PINK1 accumulation. Conversely, a significant number of fluorescent PLA spots were observed around the nucleus and within the contour of ER, and are accounted for by U2OS WT and PINK1 KO cells, when expressing recombinant PINK1-HA (figure 6*c*,*d*).

We next assessed the co-localization of PINK1-HA with other OMM Parkin substrates in U2OS PINK1 KO cells. PLA was performed with labelled Mitofusin-1 (Mfn1), VDAC and Miro1. When targeting Mfn1 and PINK1, PLA signals are nearly undetectable in both the negative control and the CCCP-treated experimental condition (figure 6*e*; electronic supplementary material, figure S6b). A similar observation is obtained when targeting Miro and PINK1 (figure 6*e*; electronic supplementary material, figure S6c). A large number of PLA signals is observed when targeting VDAC and PINK1-HA, yet these are also present in the absence of CCCP (figure 6*e*; electronic supplementary

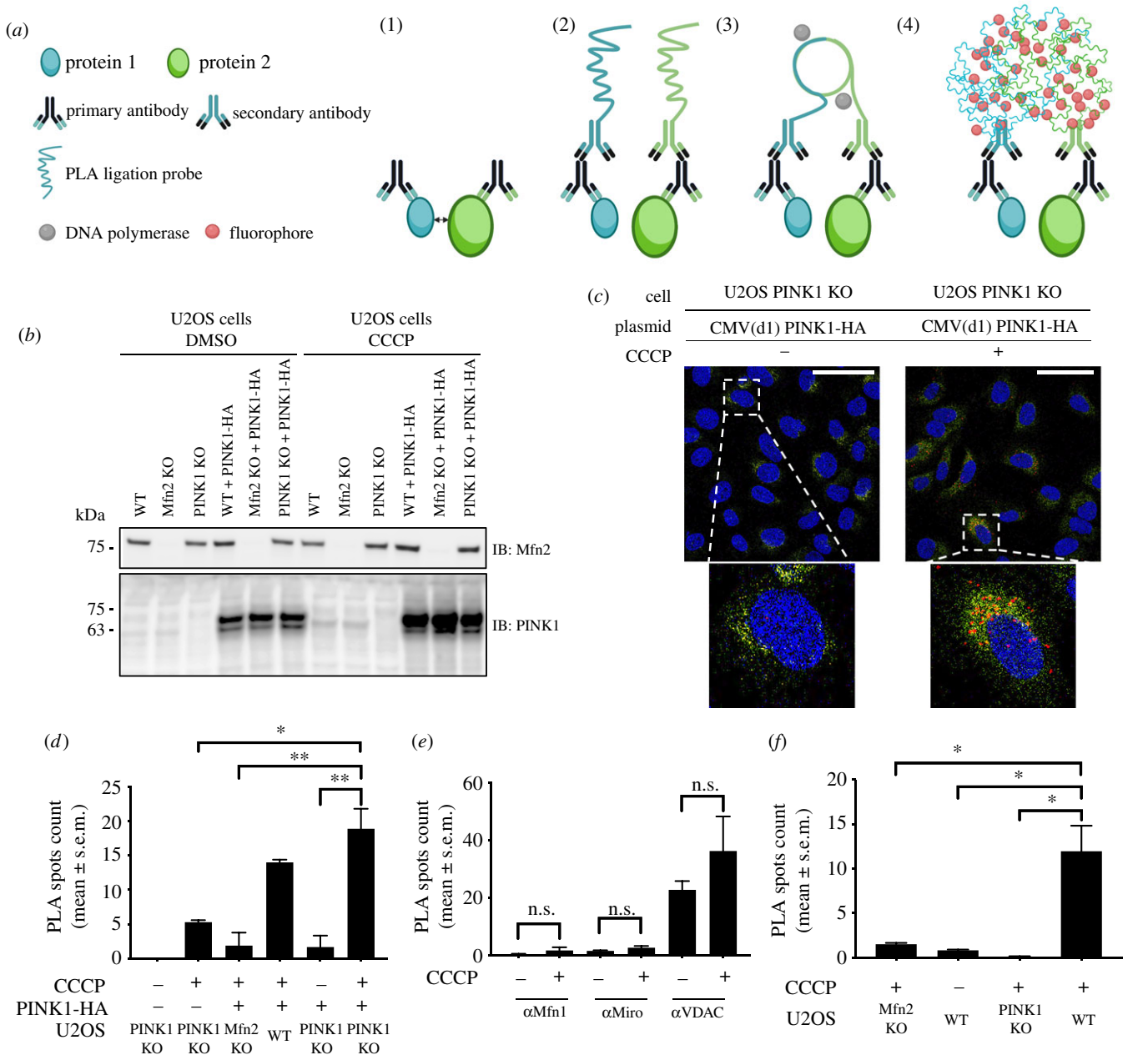

Figure 6. Co-localization of PINK1 and Mfn2 on damaged mitochondria using the PLA. (*a*) Schematic overview of PLA. (1) Two primary antibodies raised in different species recognize two proteins (less than 40 nm). (2) Secondary antibodies coupled with PLA ligation probes bind to the primary antibodies. (3) PLA ligation probes in proximity ligate to form a circular DNA template amplified by DNA polymerase. (4) Fluorophores hybridize to the template and amplify the fluorescent signals detectable by microscopy. (*b*) Immunoblots showing the Mfn2 and PINK1 expression levels in U2OS KO cells. (*c*) PLA confocal microscopy images targeting Mfn2 and PINK1-HA in U2OS PINK1 KO cells. PLA spots (red) are located around the nuclei (DAPI stain, blue) and within the contour of the ER (Alexa488-coupled anti-calnexin, green). Scale bar, 10 microns. (*d–f*) Quantification of PLA spots per cell for interactions (*d*) between Mfn2 and PINK1, (*e*) between Mfn1, MIRO or VDAC, and PINK1, and (*f*) between Mfn2 and pUb. Data from three independent experiments was tested for significance with independent *t*-tests with Bonferroni corrections post hoc test were performed. The vertical bars represent s.e.m. n.s., not significant; $*p < 0.05$; $**p < 0.01$.

material, figure S6d). In sum, none of the three tested OMM proteins are located or enriched in close proximity to PINK1 upon mitochondrial depolarization.

To further consolidate our observation, we sought to assess whether Mfn2 is found in close proximity to pUb, which is the direct output of PINK1's catalytical activity. PLA assays were performed without employing an ectopic overexpression system (i.e. transfecting exogenous PINK1-HA) to evaluate the interaction between proteins of interest at endogenous levels of PINK1 in cells. The total number of detected PLA spots show that Mfn2 is also found in proximity to pUb in cells as these signals are absent in Mfn2 KO, PINK1 KO or untreated control conditions (figure 6*f*; electronic supplementary material, figure S6e,f). Collectively, these data demonstrate that Mfn2 preferentially localizes in close proximity to PINK1 and pUb.

3. Discussion

The formation of an isopeptide bond by HECT or RBR ligases involves the transfer of the ubiquitin carboxy terminus from a cysteine thiol on the ligase to a substrate amino group. As these residues are mostly protonated at physiological pH,

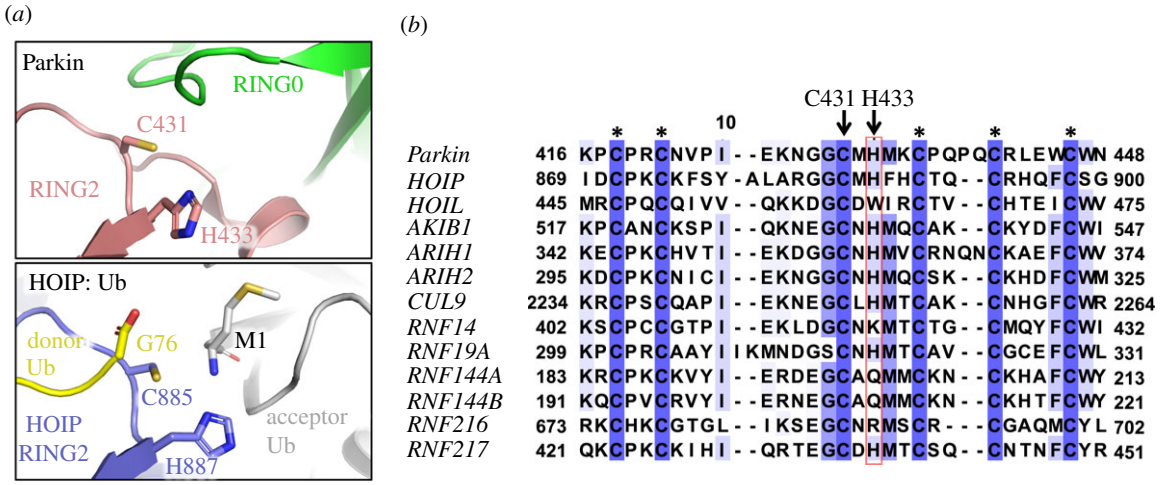

Figure 7. Conservation and structure of Parkin His433. (*a*) Comparison of the RING2 domains from auto-inhibited Parkin (pdb 4K7D) and HOIP bound to donor and acceptor ubiquitin molecules (pdb 4LJO). Met1 of the acceptor Ub is close to His887 in HOIP, which act as a general base by deprotonating the terminal amino group [33]. The C-term of the donor Ub is close to the catalytic cysteine, mimicking the Ub–Cys885 thioester intermediate. The RING0 domain in Parkin overlaps with the acceptor Ub in the HOIP complex. (*b*) Sequence alignment of RING2 domains from different human RBR E3 ubiquitin ligases. Asterisks indicate zinc-coordinating residues.

catalysis of deprotonation will lead to efficient acyl transfer. Our data show that His433 plays an important role in the acyl transfer of Ub to substrates (figures 1 and 2), consistent with those obtained for HOIP [42]. The structure of HOIP bound to ubiquitin (in both donor and acceptor position) shows the acceptor Ub bound to RING2, with its amino terminal Met1 group positioned adjacent to Cys885 and His887, while Gly76 from the donor Ub is bound to Cys885 (figure 7*a*). Cys431 and His433 in the Parkin inactive structure are oriented in a similar manner, with the RING0 domain occupying the position of the acceptor Ub in HOIP. Upon phosphorylation of the Ubl, the RING2 domain dissociates from RING0, which would allow Cys431 to form a thioester bond with a donor Ub and transfer it to an acceptor substrate amino group. One key difference between HOIP and Parkin is that the RING2 domain in HOIP is followed by a zinc finger and the linear ubiquitin chain-determining domain (LDD), which form contacts with the acceptor Ub and are essential for dictating chain specificity [54]. Parkin lacks such elements, which could explain its lack of substrate selectivity.

While His887 in HOIP is important to catalyse Ub acyl transfer, a subsequent structure of HOIP in complex with a charged E2–Ub conjugate showed that His887 also mediates hydrogen bonds with the E2 enzyme [55]. However, these interactions do not appear to be critical, since the HOIP H887A mutant can still catalyse Ub thioester transfer from an E2 [42]. While there is no structure of Parkin bound a to a charged E2–Ub conjugate, our discharging assays (figure 2) suggest that Parkin His433 is not critical for the interaction with the E2–Ub conjugate.

Intriguingly, a sequence alignment of the RING2 domain from RBR ligases shows that the Parkin His433 residue is conserved, but is not found in HOIL-1, RNF14, RNF144A/B and RNF216 (figure 7*b*). In HOIL-1, the catalytic histidine residue is replaced by Trp462. HOIL-1 binds to HOIP and is required for activation of the latter, but HOIL-1 alone does not catalyse the formation of free ubiquitin chains, contrary to the HOIP catalytic domain [56]. However, HOIL-1 is capable of generating ubiquitin chains via formation of hydroxylamine-sensitive oxyester bonds, in a reaction that is dependent on the active site Cys460 [57]. Thus, HOIL-1 has different catalytic requirements than other ligases that catalyse isopeptide bonds. RNF216 does generate polyUb chains in a Cys-dependent manner, but it's unknown whether these chains are found on lysine residues or not [58]. However, it has an arginine residue at the position equivalent to His433, and thus perhaps RNF216 catalyses acyl transfer in a different manner. Finally, RNF144A/B have a glutamine at the equivalent position and can catalyse the formation of Lys6, Lys11, Lys48 and Lys63 polyUb chains [59], again suggesting that there are different modes of acyl transfer catalysis.

It is important to note that other factors than His433 contribute to acyl transfer in Parkin. The local environment (electrostatics, solvent accessibility) of the RING2–Ub conjugate may itself lower the pKa of the side-chain amino group of lysine, which will enhance its reactivity. Indeed, we observe that the H433A mutant, while impaired, can still transfer Ub to substrates *in vitro*, to a greater extent than the C431S mutant (figures 1 and 2). For example, single-turnover reactions with UbcH7–FluoUb show that the W403A-H433A mutant still forms DTT-resistant Ub adducts on Parkin (15% compared to W403A), whereas W403A-C431S does not (figure 2*b*). Likewise, the W403A-H433A mutant is still able to form the 5-FAM-Lys-Ub adduct, with a relative activity of 20% compared to W403A after subtracting signal in the absence of Parkin (figure 1*d*). Thus, the mutation of His433 does not abolish, but rather reduces the rate of acyl transfer by 5- to 10-fold.

Furthermore, we found that the mutant H433F could still be recruited to mitochondria and induce mitophagy, albeit more slowly (figure 3). These observations go hand in hand with the proposed positive feedback mechanism where new Parkin-made Ub-chains on mitochondria are phosphorylated by PINK1 which in turn recruit more Parkin and leads to further Ub-chain synthesis [43]. In this way, when Parkin H433F fails to efficiently transfer Ub to a substrate, it also reduces the ability to boost further ligase recruitment, impairing the ability to undergo mitophagy. On immunoblots, we noticed that substrates such as Mfn1 and Mfn2 were

ubiquitinated by Parkin H433F, but compared to WT, the extent of the disappearance of the unmodified band (via degradative pathways such as the ubiquitin-proteasome pathway or mitophagy) was slightly slower (figure 3*b*). To better understand this and separate the effect of ubiquitination from either PINK1 build up or subsequent degradation pathways, we performed *in organello* ubiquitination assays on isolated mitochondria. We observed that Mfn2 ubiquitination was not affected by the His433 mutation (figure 4*b*; electronic supplementary material, figure S2a,b), whereas overall ubiquitination levels were affected by the mutation (electronic supplementary material, figure S2b). We interpret these results by proposing that the rate-limiting step for Mfn2 ubiquitination is thioester formation (His433-independent), whereas acyl transfer is the rate-limiting step for other substrates (His433-dependent). The rate of thioester formation itself depends on a multitude of upstream steps, such as Parkin binding to pUb, phosphorylation of the Ubl and release of the REP, charging of Ub on the E2 enzyme and binding of the charged E2–Ub conjugate, but critically, all of those steps are independent of the substrate. This implies that acyl transfer must be faster for Mfn2 than for other substrates (more than 5-/10-fold, based on estimation of residual *in vitro* activity by the H433A mutant), which explains why Mfn2 is the most extensively ubiquitinated substrate in our *in organello* assay (figure 4*d*).

Using quantitative mass spectrometry experiments, Ordureau *et al.* [45] estimated that Mfn2 is 100 and 25 times less abundant than VDAC1 and VDAC3 in HeLa cells, respectively. After 1 h of oligomycin/antimycin A (OA) treatment in these cells expressing Parkin, the fractional occupancy of the most abundant Lys-Gly-Gly site in VDAC3 (Lys109) is around 0.5, with around 1375 fmol of peptide per 1.5 mg of isolated mitochondria. If we extrapolate to the most kinetically favoured Mfn2 site Lys416 (55 fmol for the same amount of mitochondria, i.e. approximately 25× less than $VDAC3^{K109}$), we calculate a fractional occupancy of approximately 0.5 for $Mfn2^{K416}$, which is consistent with visual observation on immunoblots [45]. However, after only 15 min of OA treatment, the fractional occupancy has already reached approximately 0.17 for $Mfn2^{K416}$, whereas it reaches only 0.016 and 0.007 for $VDAC3^{K53}$ and $VDAC3^{K109}$, respectively. Data extracted from a recent quantitative proteomics in mouse neurons also reveal that Mfn2 is 200-fold less abundant than VDAC1, and $Mfn2^{K416}$ is one of the preferred sites of Parkin ubiquitination [60]. The data also show that the concentration of endogenous Parkin in neurons is around 60 nM, which is similar to the concentrations we have used in our *in organello* assays. Another study used a substrate-trapping method to identify Parkin substrates and again found Mfn2 as well as TOM70 as the top two substrates [61]. Those results are consistent with our own and highlight that Mfn2 is a kinetically preferred substrate of Parkin.

What, then, makes acyl transfer of Ub from Parkin to Mfn2 so efficient? We reported that Mfn2 co-purifies with pUb in cells, consistent with Mfn2 being conjugated to pUb [46]. These Mfn2-pUb conjugates would recruit Parkin selectively to mitochondrial sites enriched for Mfn2 and PINK1, thus enabling Parkin phosphorylation and bringing Parkin in closer proximity to lysine residues in Mfn2 than in other substrates. We therefore developed an artificial GST-pUb substrate to test whether coupling to pUb conferred a kinetic advantage for Parkin ubiquitination (figure 5). While Parkin binding to pUb does enhance its autoubiquitination activity, phosphorylation of its Ubl has a much stronger effect (figure 5, compare lanes 6 and 8) [32]. Yet, phospho-Parkin was unable to ubiquitinate GST-Ub, in contrast with GST-pUb which was substantially modified by Ub chains on the GST moiety because it recruits phospho-Parkin (figure 5, lanes 11 and 12). It is worth noting that for this assay, we used low concentrations of Parkin (200 nM), similar to those used *in organello*, in order to reduce autoubiquitination in *trans* via intermolecular interactions. Yet, we found that phospho-Parkin still autoubiquitinates, especially so in the absence of GST-pUb. This is probably due to the fact that there is a limited supply of Ub in the assay; addition of a kinetically preferred substrate such as GST-pUb drives the pool of Ub away from autoubiquitination towards GST ubiquitination. Yet, while binding to pUb is certainly critical for substrate ubiquitination, we cannot exclude that additional elements may contribute to substrate selectivity, such as direct interaction between phospho-Parkin and Mfn2.

Our model of Mfn2 ubiquitination by Parkin, based on proximity to pUb, implies that PINK1 must be in close proximity to Mfn2 (figure 8). Chen & Dorn [49] previously showed that Mfn2 is phosphorylated by PINK1. This enables Parkin to interact with Mfn2, although it's unclear whether these observations depend on Mfn2 being charged with pUb, as this study was conducted prior to the discovery of pUb. This proximity is also supported by our *in organello* assays using non-denaturing detergents, which abrogate Parkin's ability to ubiquitinate Mfn2 (figure 4*b*). NP40 treatment would dissolve mitochondrial membranes and position PINK1 and pUb-labelled substrates on distinct micelles, thus decoupling pUb binding from PINK1-mediated phosphorylation of Parkin. However, we cannot exclude that NP40 impairs PINK1's kinase activity, dissociates PINK1 from TOM or affects the availability of Mfn2's ubiquitination sites. On the other hand, our PLA data clearly shows that PINK1-HA and Mfn2 indeed form distinct spots in response to mitochondria depolarization (figure 6). While we also observe slightly more spots per cell between VDAC and PINK1-HA, VDAC paralogs are 25–100 more abundant than Mfn2 (in HeLa cells and neurons [45]), and therefore we expect to see many more non-specific PLA spots, and indeed we observe as many spots in cells that were not treated with CCCP (figure 6*e*). However, we cannot rule out non-specific antibody background for VDAC. The number of spots between Mfn2 and pUb was found to be in the same range as Mfn2 and PINK1-HA in cells treated with CCCP (compare figure 6*d*,*f*), suggesting that the number of spots is limited by the low abundance of Mfn2. Yet, nearly no spots were observed in cells expressing PINK1-HA but not treated with CCCP (figure 6*d*), even though these cells overexpress PINK1-HA at far higher levels than endogenous PINK1 (figure 6*b*). This suggests that only a small fraction of overexpressed PINK1-HA localizes near Mfn2 in a manner similar to endogenous PINK1 in cells treated with CCCP.

The nature of the interaction between Mfn2 and PINK1 is unknown, but several studies point to the two proteins being in close proximity at mitochondria-ER (mito-ER) contact sites [62]. Mfn2, but not Mfn1, localizes to mito-ER contact sites and tethers the two organelles [53]. Parkin-mediated ubiquitination and degradation of Mfn2 regulates formation and dissociation of mito-ER contact sites, which itself regulates

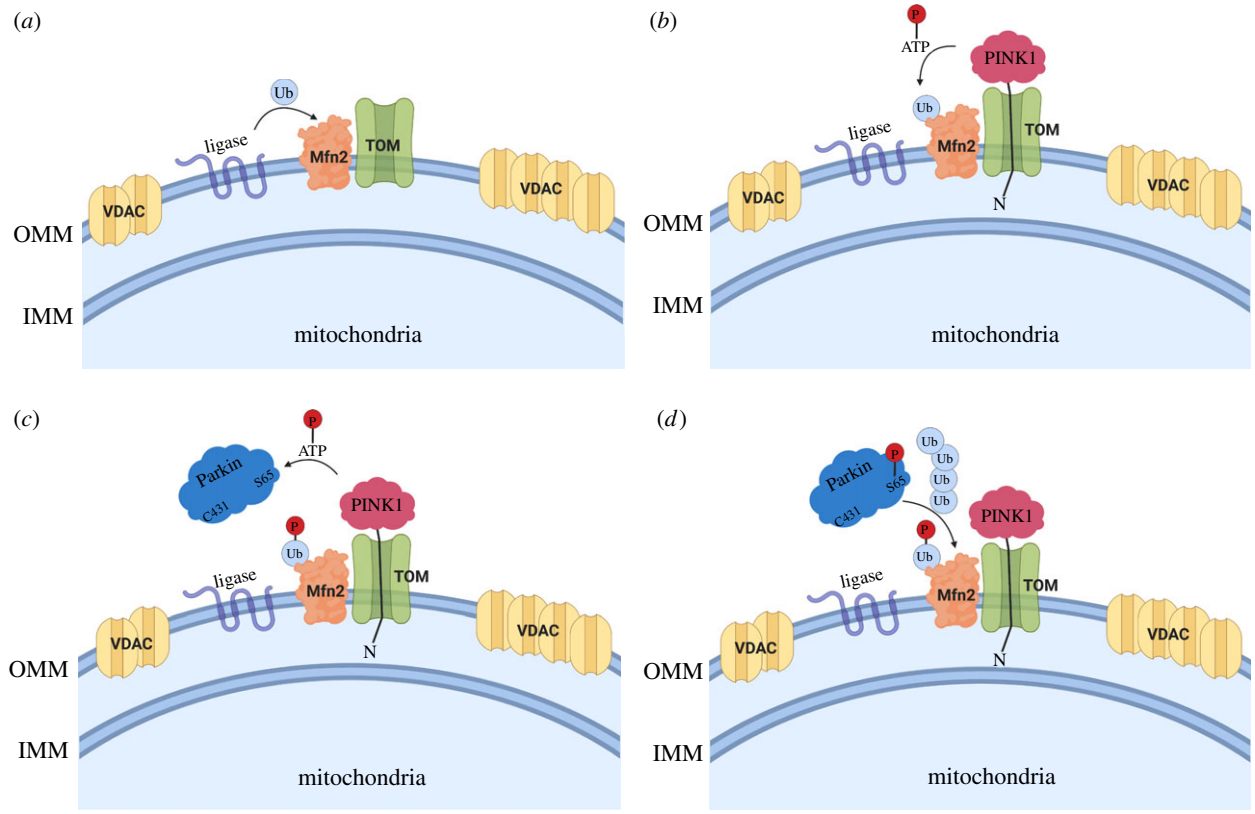

Figure 8. Schematic illustrating Parkin's substrates specificity towards Mfn2 at the onset of cellular damage. (*a*) Mitochondrial E3 Ub ligases (e.g. March5) catalyse the addition of a 'seed' Ub onto Mfn2. (*b*) PINK1 is recruited to the damaged OMM and uses its kinase activity to phosphorylate the existing Ub moieties on the nearby Mfn2. (*c*) The generation of pUb recruits Parkin, which becomes catalytically active upon phosphorylation at Ser65 by PINK1. (*d*) Parkin further catalyses the addition of Ub moieties onto Mfn2, which in turn are phosphorylated by PINK1, and the feedback loop continues. Eventually, other abundant OMM substrates such as VDAC will be ubiquitinated.

the rate of mitophagy [46,63]. PINK1 has also been shown to localize specifically at these contact sites during mitophagy [64]. While our PLA images do not allow quantification of co-localization between PINK1-Mfn2 spots and ER-mito contact sites, most PLA spots are within the ROI defined by the ER in every cell (figure 6). PINK1 would therefore accumulate specifically at ER-mito contact sites and may phosphorylate the pool of Mfn2-Ub on the ER as well as mitochondria. Intriguingly, PINK1 was observed to form a 750 kDa complex with a subset of all TOM complexes, which may correspond to TOM complexes found at ER-mito contact sites [8]. We have recently elucidated the mechanism of PINK1 autophosphorylation through dimerization and binding to the TOM complex [65], but the features of PINK1 that dictate localization at distinct TOM complexes remain undetermined and may depend on its messenger RNA or specific features of its MTS.

What would be the physiological consequences of Parkin's preference for Mfn2? Like PINK1 itself [66], ER-mito contact sites are critical for calcium homeostasis [63] and are implicated in regulating mitochondrial fission [67]. In a recent publication, fission events linked to degradation by mitophagy were shown to take place at the periphery of mitochondria, in a process involving machineries distinct from midzone fission [68]. While Parkin was recruited specifically at the periphery, it is unknown whether PINK1 and Mfn2 also localize at the periphery. Furthermore, PINK1/Parkin are not required for basal mitophagy in Drosophila and mice, but rather mediate selective turnover of a subset of mitochondrial proteins [69,70]. The mechanisms of selective turnover could involve 'bit-by-bit' mitophagy or formation of MDVs [24,71], which all rely on specific membrane fusion/fission events that are regulated by Mfn2. Importantly, these processes take place in the absence of cell-wide depolarization induced by CCCP or O/A treatment, which leads to sustained Parkin activation and ubiquitination of OMM proteins that would otherwise not be ubiquitinated under more circumscribed forms of damage. For example, stimuli such as the formation of localized aggregates on mitochondria lead to the transient activation of PINK1 and Parkin and induces a more selective mitophagy that depends on mitochondrial fission [72]. Given that Mfn2 is one of the most rapidly ubiquitinated proteins following Parkin activation, it will be critical to determine the impact of PINK1/Parkin-mediated Mfn2 ubiquitination in these settings.

We have previously shown that pUb chains build up on mitochondria in the absence of Parkin, and that binding to these so-called 'pre-existing' pUb chains is required for Parkin phosphorylation and activation [35]. If PINK1 phosphorylates Ub located on OMM proteins such as Mfn2 prior to Parkin recruitment, which E3 ubiquitin ligase(s) ubiquitinate(s) Mfn2 in the first place? In addition to Parkin, a number of ubiquitin ligases have been shown to ubiquitinate Mfn2, including Huwe1, Mul1, March5 and Gp78 [62]. Huwe1 is a cytosolic HECT-type Ub ligase that forms Lys6-Ub chains and can ubiquitinate Mfn2 in cells [59,73]. Mul1, also known as MAPL, is a membrane protein with a RING domain that bears ubiquitination as well as sumoylation activity and has been reported to modulate Mfn2 [74,75].

March5, also known as MITOL, is an integral membrane protein on the OMM that harbours a RING domain and ubiquitinates Mfn2 [76,77]. The group of Noriyuki Matsuda knocked down all three Ub ligases and found that only March5 knockdown affected Parkin-dependent substrate ubiquitination [78]. Furthermore, they showed that March5 KO attenuated Parkin recruitment to depolarized mitochondria, whereas March5 overexpression accelerated recruitment. The group of Wade Harper later showed that KO of Mul1 or March5 did not affect pUb chain formation or substrate ubiquitination 4 h after depolarization [79], which is still consistent with the observations by the Matsuda laboratory, who showed that Parkin recruitment is not affected by March5 KO after more than 90 min depolarization [78]. Phu *et al*. [80] later showed that knockdown of March5 reduces overall the level of pUb chains after 4 h depolarization, in HeLa cells lacking Parkin. This group also found that the deubiquitinase Usp30 opposes the effect of March5 on the ubiquitination of proteins imported to mitochondria, and Ups30 KO in HEK293 cells increased pUb levels. Thus, March5 at the very least modulates Parkin-dependent mitochondrial protein turnover and may be critical to prime the Parkin-PINK1 pathway in a physiological context. Intriguingly, March5 also regulates mito-ER contact sites [81]. Finally, the E3 ligase Gp78, which is involved in ER-associated degradation, also ubiquitinates Mfn1/Mfn2 and may also regulate pathway initiation at ER-mito contact sites [82].

In conclusion, our work demonstrates that Parkin preferably ubiquitinates Mfn2 by virtue of its proximity to PINK1 on the mitochondrial outer membrane. Future work should determine the nature and location of the PINK1 : Mfn2 interaction, the mechanism and physiological triggers that lead to the formation of pUb-labelled Mfn2, and the role of March5 and other ubiquitin ligases in priming the Parkin-PINK1 pathway.

4. Material and methods

4.1. Cloning and production of purified recombinant proteins

Synthetic codon optimized (DNA Express Inc.) genes of *Rattus norvegicus* Parkin and *Dendroctonus ponderosae* PINK1 (123–570) for *E. coli* expression were cloned into pGEX-6P-1 using BamH1 and Xho1 restriction enzymes. Single-point mutations were introduced using PCR site-directed mutagenesis. Protein expression in BL21 (DE3) *E. coli* cells were induced with 25 µM isopropyl-β-D-thiogalactoside (IPTG) for the different Parkin variants and 100 µM IPTG for DpPINK1. Protein purification was performed as previously described [32]. Briefly, proteins were purified by glutathione-Sepharose agarose affinity and eluted with 20 mM glutathione, followed by 3C cleavage and size-exclusion chromatography on Superdex 200 16/60 (GE Healthcare) in 50 mM Tris-HCl pH 7.5, 120 mM NaCl, and 1 mM DTT or 0.5 mM TCEP. His6-tag UbcH7 was produced in BL21 (DE3) *E. coli* cells transformed with pET28a-LIC-UbcH7 [27]. Protein was purified by Ni-NTA (Qiagen) and eluted with 300 mM Imidazole, followed by gel filtration on Superdex 75 16/60 (GE Healthcare) in 10 mM HEPES pH 7.5, 50 mM NaCl and 1 mM DTT. Protein concentrations were determined with ultraviolet absorption at 280 nm using the theoretical extinction coefficients.

4.2. In vitro phosphorylation of proteins by *Dp*PINK1

Parkin phosphorylation was performed with 3.5 µM GST-*Dp*PINK1 and 20 µM of *Rn*Parkin (in 50 mM Tris-HCl, 120 mM NaCl and 1 mM DTT), 10 mM $MgCl_2$ and 1 mM ATP in a reaction volume of 20 µl at 30°C for 30 to 60 min. GST fused to ubiquitin (GST-Ub) phosphorylation was performed with 3.5 µM *Dp*PINK1 and 43 µM of GST-Ub (in 50 mM Tris-HCl, 120 mM NaCl and 1 mM DTT), 10 mM $MgCl_2$ and 1 mM ATP in a reaction volume of 20 µl at 30°C for 30 to 60 min. Phosphorylated proteins were recovered by gel filtration on Superdex 200 Increase (GE Healthcare) in 50 mM Tris-HCl, 120 mM NaCl pH 7.5. Protein concentrations were determined with ultraviolet absorption at 280 nm using the theoretical extinction coefficients. Phosphorylation was confirmed using intact mass spectrometry.

4.3. Autoubiquitination and fluorescent lysine ubiquitination assays

The autoubiquitination assays (figure 1*c*) were performed at 37°C for 120 min, in 50 mM Tris-HCl pH 7.5, 120 mM NaCl, 1 mM DTT, 2 mM ATP, 50 µM Ub (Boston Biochem), 10 mM $MgCl_2$, 50 nM E1 (Boston Biochem), 2 µM UbcH7 and 1.5 µM GST-*Rn*Parkin. Reactions were stopped with the addition of SDS-PAGE sample buffer containing 50 mM DTT and analysed using SDS-PAGE and Coomassie Brilliant Blue (CBB) staining. For the experiment shown in the electronic supplementary material, figure S2c, the same conditions were used, but Tris-HCl and NaCl were replaced by mitochondrial isolation buffer (20 mM HEPES/KOH pH 7.4, 220 mM mannitol, 10 mM potassium acetate and 70 mM sucrose), with or without 0.1% NP-40. The ubiquitination assay with fluorescent lysine (figure 1*d*) was performed at 37°C for 60 min, in 50 mM HEPES pH 7.4, 50 mM NaCl, 0.5 mM DTT, 2 mM ATP, 50 µM Ub, 10 mM $MgCl_2$, 50 nM E1 4 µM UbcH7, 2 µM GST-*Rn*Parkin and 1 mM 5-FAM-Lysine (Anaspec), prepared from a 20 mM stock in DMSO. Reactions were stopped SDS-PAGE sample buffer containing 50 mM DTT and analysed using SDS-PAGE and fluorescence imaging (Cy2 channel).

4.4. Charging and discharging assays of UbcH7

Ten micrograms of ubiquitin-conjugating enzyme, UbcH7, were charged with 10 µg ubiquitin or N-terminally fluorescein-labelled Ub (FluoUb, Boston Biochem) using 0.02 µg ubiquitin-activating enzyme (His6-E1, Boston Biochem Inc.), 0.5 mM ATP and 10 mM $MgCl_2$ in 50 mM Tris-HCl pH 7.4, 120 mM NaCl and 1 mM TCEP, in a 100 µl reaction. Reactions were performed at 37°C at different time points to a maximum of 60 min.

Ubiquitin-loaded UbcH7 (0.8 µg UbcH7–Ub or UbcH7–FluoUb) was mixed with 1.2 µg of *Rn*Parkin (in 50 mM Tris-HCl pH 7.4, 120 mM NaCl and 1 mM TCEP). Mixtures were incubated at 30°C for up to 40 min to monitor discharging (figure 2*a*,*c*). Reactions were stopped with the addition of SDS-PAGE sample buffer containing 12 mM TCEP, resolved on SDS-PAGE and analysed using the Typhoon

fluorescent scanner (GE), Coomassie staining, silver staining (Thermo Pierce kit) or transferred to a nitrocellulose membrane and probed with mouse anti-ubiquitin (Covance, 1 : 10 000) and detected with Clarity Lightning ECL (Bio Rad). Images acquired with an ImageQuant LAS 500 (GE Healthcare). Densitometry and fluorescence intensity analysis was performed using Fiji [83].

4.5. Fluorescent-ubiquitin charging assay on Parkin

Eight micromolar of UbcH7 was charged with 10 µM N-terminal fluorescein-labelled Ub at 37°C for 15 min in 50 mM HEPES pH 7.4, 50 mM NaCl, 0.5 mM TCEP, 4 mM ATP, 2 mM $MgCl_2$ and 100 nM E1 (figure 2*b*). The master mix was then split and mixed with an equivalent volume of GST-RnParkin WT or mutants (4 µM) and incubated at 37°C for 15 min. Each reaction was split and stopped with SDS-PAGE sample buffer containing either 50 mM TCEP or 100 mM DTT. Reactions were resolved on SDS-PAGE and analysed using fluorescence imaging (Cy2 channel).

4.6. Ubiquitination of GST-ubiquitin/phospho-ubiquitin

Ubiquitination assays (figure 5*b*) were performed at 37°C for 30 min, in buffer containing 50 mM Tris-HCl pH 8.0, 5 mM $MgCl_2$, 4 µM UbcH7 or UbcH7–Ub (charged as described above), 0.1 µM *Rn*Parkin or phosphorylated *Rn*Parkin (Parkin^{S65}), 50 µM TCEP and 2 µg of GST-Ub or phosphorylated GST-Ub (GST-pUb^{S65}). Reactions were stopped with the addition of SDS-PAGE sample buffer containing 100 mM DTT and analysed using gel electrophoresis and CBB staining or immunoblotting. The same reactions (conditions in lanes 9–12 in figure 5*b*) were repeated and frozen at −80°C for digestion and mass spectrometry (figure 5*c*) or SDS-PAGE analysis (electronic supplementary material, figure S3c).

4.7. Cell culture, mammalian plasmid DNA and generation of stable cell lines

U2OS and HeLa cell lines were maintained at 37°C and 5% CO2 in Dulbecco's modified Eagle's medium (DMEM) with 10% fetal bovine serum, 2 mM glutamine, 0.1% penicillin and 0.1% streptomycin (Wisent Life Sciences). Parkin mutant plasmids were cloned beginning with a *Homo sapiens* WT eGFP-Parkin vector [44] and performing PCR point mutagenesis (Quikchange Mutagenesis kit: Stratagene) using primers ordered from Invitrogen. Mutations were verified by sequencing at the Genome Québec Facility.

Plasmid DNA was introduced into U2OS cells following a protocol for jetPrime transfection reagent (Polyplus). Nucleic acid was first diluted in jetPrime buffer (Polyplus) and combined with jetPrime transfection reagent before being added to U2OS cells immersed in fresh DMEM. Cells were incubated overnight in the transfection mix and allowed to express eGFP-Parkin constructs, a process that was verified by fluorescent light microscopy. The selection of cells stably expressing eGFP-Parkin WT and mutant constructs was accomplished by maintaining them in DMEM laced with 200 mg l^{-1} G418 (Multicell). U2OS cells were grown in G418-DMEM for a period of approximately two weeks and passaged using trypsin as necessary.

4.8. Mitochondrial Parkin recruitment, mitophagy assay and fluorescence microscopy

DMEM containing CCCP at a final concentration of 20 µM, or 0.1% DMSO, was added to plates growing GFP-Parkin-expressing U2OS cells for 1, 2, 4 or 24 h. For immunoblots, cells were harvested on ice in cold phosphate-buffered saline (PBS). Cells were washed and lysed in RIPA buffer with a protease inhibitor cocktail (1 : 100 benzamidine, 1 : 10 000 aprotinin, 1 : 10 000 leupeptin, 1 : 500 PMSF). Protein concentration in these samples was quantified using the Pierce BCA Assay (Thermo Scientific). Samples were mixed with SDS-PAGE sample buffer with 100 mM DTT and resolved by SDS-PAGE. Proteins were transferred to a nitrocellulose membrane and stained with ponceau. After staining, membranes were washed with PBS-0.1% Tween 20 (PBS-T), blocked with 5% milk/PBS-T and incubated with primary antibodies overnight. Primaries used in all experiments included mouse anti-Parkin (1 : 20 000; Santa Cruz), rabbit anti-Mfn1 and anti-Mfn2 (1 : 2000, Santa Cruz) and mouse anti-VDAC1 (1 : 10 000, Abcam) diluted in PBS-T with 3% BSA. Bound protein was detected on film using HRP-coupled secondary antibodies (donkey- or goat- anti-rabbit/anti-mouse), treated with Western Lightning ECL/Super ECL as needed (Perkin Elmer).

For microscopy, cells grown on coverslips were fixed with 4% formaldehyde-PBS (prepared from 16% formaldehyde stock, Thermo Fisher Scientific) for 15 min at 37°C. After fixation, cells were washed four times with 1 × PBS, permeabilized with 1 × PBS containing 0.25% Triton X-100 for 10 min and blocked with 3% BSA + PBST (1 × PBS + 0.1% Tween-20) for 1 h at RT. Cells were incubated overnight at 4°C with rabbit anti-Tom20 (1 : 1000, Santa Cruz) followed by Alexa Fluor 555 donkey anti-rabbit (Invitrogen). Cells were washed three times in PBS, and coverslips were mounted with fluorescent mounting medium (Dako). Confocal images were acquired on an LSM 510 Meta confocal microscope (Zeiss) using a 25×, 0.8 NA or 63×, 1.4 NA objective. Excitation wavelengths of 488 nm (GFP-Parkin) and 633 nm (Tom20) were used. For quantification, slides were blinded for three independent experiments and 100 cells were counted per experiment. Cells were analysed for the number of cells with Tom20 staining (CCCP 24 h), the number of cells with GFP-Parkin co-localization on Tom20-positive mitochondria (CCCP 1–2 h), or for the number of cells containing GFP-Parkin puncta or aggregates co-localizing with Tom20-positive mitochondria (CCCP 24 h).

4.9. Mitochondria isolation and *in organello* ubiquitination assay

HeLa cells treated with 10 µM CCCP or DMSO for 3 h were suspended in mitochondrial isolation buffer (20 mM HEPES/KOH pH 7.4, 220 mM mannitol, 10 mM potassium acetate and 70 mM sucrose) on ice. Cells were disrupted by nitrogen cavitation and cell homogenates were centrifuged at 600*g* for 5 min at 4°C to obtain a post-nuclear supernatant. Cytosolic fractions were collected by two further centrifugation steps for 10 min at 4°C, the first at 10 000 g and the second at 12 000*g*. Mitochondria pellets were suspended in mitochondria isolation buffer to a concentration of 2 mg ml^{-1} and stored at −80°C until further use. Forty

micrograms of CCCP- or DMSO-treated mitochondria were supplemented with an ubiquitination reaction mix (20 nM E1, 100 nM of UbcH7, 5 µM ubiquitin, 1 mM ATP, 5 mM $MgCl_2$ and 50 µM TCEP in mitochondria isolation buffer) and 100 nM of recombinant *Rn*Parkin in a 40 µl reaction. After a 30 min incubation at 37°C, reactions were stopped with 3 × sample buffer with 100 mM DTT and analysed by western blotting. Reactions were loaded on 8% tris-glycine. Proteins were transferred to nitrocellulose and stained with Ponceau. Membranes were blocked with 5% milk in PBS-T (0.1% Tween 20) and incubated with rabbit anti-mitofusin 2 (mAb D2D10, Cell Signaling), rabbit anti-mitofusin 1 (mAb 13196S, Cell Signaling), rabbit anti-Miro1 (mAb 14016S, Cell Signaling), rabbit anti-HK1 (mAb C35C4, Cell Signaling), rabbit anti-HK2 (mAb C64G5, Cell Signaling), rabbit anti-Tom20 (pAb FL-145, Santa Cruz Biotechnology), rabbit anti-Tom70 (pAb C-18, Santa Cruz Biotechnology), mouse anti-Parkin (mAb Prk8, Cell Signaling), rabbit anti-PINK1 (mAb D8G3, Cell Signaling), mouse anti-Ub (mAb P4D1, Cell Signaling), rabbit anti-phospho-ubiquitin S65 (Millipore), rabbit anti-PDH (mAb C54G1, Cell Signaling) or rabbit anti-VDAC (mAb D73D12, Cell Signaling) diluted in PBS-T with 3% bovine serum albumin (BSA). Membranes were washed with PBS-T and incubated with HRP-coupled goat anti-mouse or anti-rabbit IgG antibodies (Cell Signaling). Detection was performed with Clarity Lightning ECL (Bio Rad) and images acquired with an ImageQuant LAS 500 (GE Healthcare).

4.10. Proximity-ligation assay for proteins interaction studies

Protein–protein interactions were analysed using Duolink *in situ* orange starter fluorescence kit (mouse/rabbit, Sigma-Aldrich) in human osteosarcoma U2OS cells (WT, Mfn2 KO and PINK1 KO). Cells were grown to confluency on coverslips (Fisherbrand) and 5 µg pCMV(d1) TNT PINK1(WT)-3HA plasmids, obtained from Noriyuki Matsuda for attenuated PINK1 expression, were transfected using Lipofectamine 3000 Reagent (ThermoFisher Scientific). Cells were grown for an additional 48 h post transfection. Cells were treated with 10 µM CCCP or DMSO for 3 h before fixation and permeabilization using 4% PFA/0.1% Triton-X-100 for 10 min at room temperature. Samples were blocked using Duolink blocking solution in a preheated humidified chamber at 37°C for 1 h. Primary antibody solution mix contains two primary antibodies raised in two different species (mouse and rabbit) targeting the proteins of interest: rabbit anti- mitofusin 2 (1 : 50, mAb D2D10, Cell Signaling), rabbit anti-VDAC (1 : 200, mAb D73D12, Cell Signaling), mouse anti-HA (1 : 100, mAb D73D12, Cell Signaling), rabbit anti-mitofusin 1 (1 : 100, mAb 13196S, Cell Signaling), rabbit anti-Miro1 (1 : 50, mAb 14016S, Cell Signaling), rabbit anti-pUb (1 : 100, mAb 37642S, Cell Signaling) or mouse anti-mitofusin 2 (1 : 50, mAb 661–757, Abnova) was added for overnight incubation at 4°C. The next day, cells were incubated with PLA probes PLUS and MINUS diluted 1 : 5 for 1 h at 37°C. After ligation, the samples were incubated with amplification polymerase solution for 100 min at 37°C, protected from light. The ER was stained using an Alexa488-coupled anti-calnexin (1 : 200, mAb AF18, ThermoFisher Scientific) in 10% goat serum overnight at 4°C. Cell nuclei were stained using DAPI (1 : 1000, ThermoFisher Scientific) for 10 min at room temperature. All samples were mounted with mounting medium (Dako, Agilent). Images were acquired with a 40 × Plan Apo oil-immersion objective using a TCS SP8 confocal microscope (Leica). Automatic quantification of PLA spots per cell was performed by first using the Columbus Image Analysis System (PerkinElmer) to automatically define the ER ROI using the anti-calnexin Alexa488 signal. The number of PLA spots within each ROI was then counted for at least 25 cells per condition.

4.11. Protein digestion and mass spectrometry

Ubiquitination reaction samples (3 µg protein) were diluted in denaturing buffer (3 M urea, 25 mM TEAB pH 8.5, 0.5 mM EDTA) and reduced using 2 mM TCEP for 10 min at 37°C, followed by alkylation with 50 mM chloroacetamide for 30 min at room temperature in the dark. Chloroacetamide was used to avoid iodoacetamide-induced artefacts that mimic ubiquitination [84]. Samples were diluted with 50 mM TEAB pH 8.5 to 1 M urea and digested with 0.5 µg trypsin (Sigma) for 3 h at 37°C. Digested peptides were purified using C18 Spin Columns (ThermoFisher) and resuspended in 0.1% formic acid. Peptides (0.5 µg) were captured and eluted from an Acclaim PepMap100 C18 column with a 2 h gradient of acetonitrile in 0.1% formic acid at 200 ml min^{-1}. The eluted peptides were analysed with an Impact II Q-TOF spectrometer equipped with a Captive Spray nanoelectrospray source (Bruker). Data were acquired using data-dependent automatic tandem mass spectrometry (auto-MS/MS) and analysed with MaxQuant using a standard search procedure against a custom-made FASTA file including GST-Ub, Parkin, Ub and UbcH7. Methionine oxidation, Lys ubiquitination (diGly) and Ser/Thr phosphorylation were included as variable modifications. Cysteine carbamylation was included as fixed modification.

Data accessibility. All data supporting our research are included in the submission.

Authors' contributions. M.V.: conceptualization, formal analysis, investigation, methodology, project administration, writing – original draft and writing—review and editing; Y.L.: conceptualization, formal analysis, investigation, methodology, writing—original draft and writing—review and editing; S.R.: investigation, methodology and writing—review and editing; N.C.: methodology; J.D.K.: investigation and methodology; V.S.: investigation and methodology; K.G.: conceptualization, funding acquisition, supervision and writing—review and editing; E.A.F.: conceptualization, funding acquisition, supervision and writing—review and editing; T.M.D.: conceptualization, supervision and writing—review and editing; J.-F.T.: conceptualization, formal analysis, funding acquisition, investigation, methodology, project administration, supervision, writing—original draft and writing—review and editing. All authors gave final approval for publication and agreed to be held accountable for the work performed therein.

Competing interests. J.-F.T. is a member of the scientific advisory board of Mitokinin Inc.

Funding. This work was supported by a Canada Research Chair grant to J.-F.T. (grant no. 950-229792) and E.A.F. (grant no. 950-232176), as well as a Canadian Institutes of Health Research (CIHR) grants to K.G. (grant no. FDN-159903), E.A.F. (grant no. FDN-154301) and J.-F.T. (grant no. PJT-153274). We thank the Canada Foundation for Innovation for infrastructure support (no. 229792).

Acknowledgements. We thank the McGill Pharmacology SPR/MS facility (M. Hancock) and Imaging and Molecular Biology Platform (N. Audet) for assistance with experiments.

References

1. Kitada T, Asakawa S, Hattori N, Matsumine H, Yamamura Y, Minoshima S, Yokochi M, Mizuno Y, Shimizu N. 1998 Mutations in the Parkin gene cause autosomal recessive juvenile Parkinsonism. *Nature* **392**, 605–608. (doi:10.1038/33416)
2. Winklhofer KF. 2014 Parkin and mitochondrial quality control: toward assembling the puzzle. *Trends Cell Biol.* **24**, 332–341. (doi:10.1016/j.tcb.2014.01.001)
3. Valente EM *et al.* 2004 Hereditary early-onset Parkinson's disease caused by mutations in PINK1. *Science* **304**, 1158–1160. (doi:10.1126/science.1096284)
4. Greene AW, Grenier K, Aguileta MA, Muise S, Farazifard R, Haque ME, Mcbride HM, Park DS, Fon EA. 2012 Mitochondrial processing peptidase regulates PINK1 processing, import and Parkin recruitment. *EMBO Rep.* **13**, 378–385. (doi:10.1038/embor.2012.14)
5. Jin SM, Lazarou M, Wang C, Kane LA, Narendra DP, Youle RJ. 2010 Mitochondrial membrane potential regulates PINK1 import and proteolytic destabilization by PARL. *J. Cell Biol.* **191**, 933–942. (doi:10.1083/jcb.201008084)
6. Yamano K, Youle RJ. 2013 PINK1 is degraded through the N-end rule pathway. *Autophagy* **9**, 1758–1769. (doi:10.4161/auto.24633)
7. Liu Y, Guardia-Laguarta C, Yin J, Erdjument-Bromage H, Martin B, James M, Jiang X, Przedborski S. 2017 The ubiquitination of PINK1 is restricted to its mature 52-kDa form. *Cell Rep.* **20**, 30–39. (doi:10.1016/j.celrep.2017.06.022)
8. Lazarou M, Jin SM, Kane LA, Youle RJ. 2012 Role of PINK1 binding to the TOM complex and alternate intracellular membranes in recruitment and activation of the E3 ligase Parkin. *Dev. Cell* **22**, 320–333. (doi:10.1016/j.devcel.2011.12.014)
9. Narendra DP, Jin SM, Tanaka A, Suen DF, Gautier CA, Shen J, Cookson MR, Youle RJ. 2010 PINK1 is selectively stabilized on impaired mitochondria to activate Parkin. *PLoS Biol.* **8**, e1000298. (doi:10.1371/journal.pbio.1000298)
10. Matsuda N *et al.* 2010 PINK1 stabilized by mitochondrial depolarization recruits Parkin to damaged mitochondria and activates latent Parkin for mitophagy. *J. Cell Biol.* **189**, 211–221. (doi:10.1083/jcb.200910140)
11. Geisler S, Holmstrom KM, Skujat D, Fiesel FC, Rothfuss OC, Kahle PJ, Springer W. 2010 PINK1/Parkin-mediated mitophagy is dependent on VDAC1 and p62/SQSTM1. *Nat. Cell Biol.* **12**, 119–131. (doi:10.1038/ncb2012)
12. Rasool S, Soya N, Truong L, Croteau N, Lukacs GL, Trempe JF. 2018 PINK1 autophosphorylation is required for ubiquitin recognition. *EMBO Rep.* **19**, e44981. (doi:10.15252/embr.201744981)
13. Schubert AF, Gladkova C, Pardon E, Wagstaff JL, Freund SMV, Steyaert J, Maslen SL, Komander D. 2017 Structure of PINK1 in complex with its substrate ubiquitin. *Nature* **552**, 51–56. (doi:10.1038/nature24645)
14. Kumar A, Tamjar J, Waddell AD, Woodroof HI, Raimi OG, Shaw AM, Peggie M, Muqit MMK, Van Aalten DMF. 2017 Structure of PINK1 and mechanisms of Parkinson's disease associated mutations. *eLife* **6**, e29985. (doi:10.7554/eLife.29985)
15. Koyano F *et al.* 2014 Ubiquitin is phosphorylated by PINK1 to activate parkin. *Nature* **510**, 162–166. (doi:10.1038/nature13392)
16. Kane LA, Lazarou M, Fogel AI, Li Y, Yamano K, Sarraf SA, Banerjee S, Youle RJ. 2014 PINK1 phosphorylates ubiquitin to activate Parkin E3 ubiquitin ligase activity. *J. Cell Biol.* **205**, 143–153. (doi:10.1083/jcb.201402104)
17. Kondapalli C *et al.* 2012 PINK1 is activated by mitochondrial membrane potential depolarization and stimulates Parkin E3 ligase activity by phosphorylating Serine 65. *Open Biol.* **2**, 120080. (doi:10.1098/rsob.120080)
18. Narendra D, Tanaka A, Suen DF, Youle RJ. 2008 Parkin is recruited selectively to impaired mitochondria and promotes their autophagy. *J. Cell Biol.* **183**, 795–803. (doi:10.1083/jcb.200809125)
19. Sarraf SA, Raman M, Guarani-Pereira V, Sowa ME, Huttlin EL, Gygi SP, Harper JW. 2013 Landscape of the Parkin-dependent ubiquitylome in response to mitochondrial depolarization. *Nature* **496**, 372–376. (doi:10.1038/nature12043)
20. Chan NC, Salazar AM, Pham AH, Sweredoski MJ, Kolawa NJ, Graham RL, Hess S, Chan DC. 2011 Broad activation of the ubiquitin-proteasome system by Parkin is critical for mitophagy. *Hum. Mol. Genet.* **20**, 1726–1737. (doi:10.1093/hmg/ddr048)
21. Tanaka A, Cleland MM, Xu S, Narendra DP, Suen DF, Karbowski M, Youle RJ. 2010 Proteasome and p97 mediate mitophagy and degradation of mitofusins induced by Parkin. *J. Cell Biol.* **191**, 1367–1380. (doi:10.1083/jcb.201007013)
22. Ordureau A, Heo JM, Duda DM, Paulo JA, Olszewski JL, Yanishevski D, Rinehart J, Schulman BA, Harper JW. 2015 Defining roles of Parkin and ubiquitin phosphorylation by PINK1 in mitochondrial quality control using a ubiquitin replacement strategy. *Proc. Natl Acad. Sci. USA* **112**, 6637–6642. (doi:10.1073/pnas.1506593112)
23. Lazarou M, Sliter DA, Kane LA, Sarraf SA, Wang C, Burman JL, Sideris DP, Fogel AI, Youle RJ. 2015 The ubiquitin kinase PINK1 recruits autophagy receptors to induce mitophagy. *Nature* **524**, 309–314. (doi:10.1038/nature14893)
24. McLelland GL, Soubannier V, Chen CX, McBride HM, Fon EA. 2014 Parkin and PINK1 function in a vesicular trafficking pathway regulating mitochondrial quality control. *EMBO J.* **33**, 282–295.
25. Wenzel DM, Lissounov A, Brzovic PS, Klevit RE. 2011 UBCH7 reactivity profile reveals Parkin and HHARI to be RING/HECT hybrids. *Nature* **474**, 105–108. (doi:10.1038/nature09966)
26. Fiesel FC, Moussaud-Lamodiere EL, Ando M, Springer W. 2014 A specific subset of E2 ubiquitin-conjugating enzymes regulate Parkin activation and mitophagy differently. *J. Cell Sci.* **127**, 3488–3504.
27. Trempe JF *et al.* 2013 Structure of Parkin reveals mechanisms for ubiquitin ligase activation. *Science* **340**, 1451–1455. (doi:10.1126/science.1237908)
28. Wauer T, Komander D. 2013 Structure of the human Parkin ligase domain in an autoinhibited state. *EMBO J.* **32**, 2099–2112. (doi:10.1038/emboj.2013.125)
29. Riley BE *et al.* 2013 Structure and function of Parkin E3 ubiquitin ligase reveals aspects of RING and HECT ligases. *Nat. Commun.* **4**, 1982. (doi:10.1038/ncomms2982)
30. Chaugule VK, Burchell L, Barber KR, Sidhu A, Leslie SJ, Shaw GS, Walden H. 2011 Autoregulation of Parkin activity through its ubiquitin-like domain. *EMBO J.* **30**, 2853–2867. (doi:10.1038/emboj.2011.204)
31. Wauer T, Simicek M, Schubert A, Komander D. 2015 Mechanism of phospho-ubiquitin-induced Parkin activation. *Nature* **524**, 370–374. (doi:10.1038/nature14879)
32. Sauvé V *et al.* 2015 A Ubl/ubiquitin switch in the activation of Parkin. *EMBO J.* **34**, 2492–2505. (doi:10.15252/embj.201592237)
33. Kumar A *et al.* 2015 Disruption of the autoinhibited state primes the E3 ligase Parkin for activation and catalysis. *EMBO J.* **34**, 2506–2521. (doi:10.15252/embj.201592337)
34. Kazlauskaite A *et al.* 2015 Binding to serine 65-phosphorylated ubiquitin primes Parkin for optimal PINK1-dependent phosphorylation and activation. *EMBO Rep.* **16**, 939–954. (doi:10.15252/embr.201540352)
35. Tang MY, Vranas M, Krahn AI, Pundlik S, Trempe JF, Fon EA. 2017 Structure-guided mutagenesis reveals a hierarchical mechanism of Parkin activation. *Nat. Commun.* **8**, 14697. (doi:10.1038/ncomms14697)
36. Sauvé V, Sung G, Soya N, Kozlov G, Blaimschein N, Miotto L, Trempe JF, Lukacs GL, Gehring K. 2018 Mechanism of Parkin activation by phosphorylation. *Nat. Struct. Mol. Biol.* **25**, 623–630. (doi:10.1038/s41594-018-0088-7)
37. Gladkova C, Maslen SL, Skehel JM, Komander D. 2018 Mechanism of Parkin activation by PINK1. *Nature* **559**, 410–414. (doi:10.1038/s41586-018-0224-x)
38. Matsuda N, Kitami T, Suzuki T, Mizuno Y, Hattori N, Tanaka K. 2006 Diverse effects of pathogenic mutations of Parkin that catalyze multiple monoubiquitylation in vitro. *J. Biol. Chem.* **281**, 3204–3209. (doi:10.1074/jbc.M510393200)
39. Hampe C, Ardila-Osorio H, Fournier M, Brice A, Corti O. 2006 Biochemical analysis of Parkinson's disease-causing variants of Parkin, an E3 ubiquitin-protein ligase with monoubiquitylation capacity. *Hum. Mol. Genet.* **15**, 2059–2075. (doi:10.1093/hmg/ddl131)

40. Pahari S, Sun L, Alexov E. 2019 PKAD: a database of experimentally measured pKa values of ionizable groups in proteins. *Database (Oxford)* **2019**, baz024. (doi:10.1093/database/baz024)
41. Spratt DE *et al.* 2013 A molecular explanation for the recessive nature of Parkin-linked Parkinson's disease. *Nat. Commun.* **4**, 1983. (doi:10.1038/ncomms2983)
42. Stieglitz B *et al.* 2013 Structural basis for ligase-specific conjugation of linear ubiquitin chains by HOIP. *Nature* **503**, 422–426. (doi:10.1038/nature12638)
43. Ordureau A *et al.* 2014 Quantitative proteomics reveal a feedforward mechanism for mitochondrial Parkin translocation and ubiquitin chain synthesis. *Mol. Cell* **56**, 360–375. (doi:10.1016/j.molcel.2014.09.007)
44. Durcan TM *et al.* 2014 USP8 regulates mitophagy by removing K6-linked ubiquitin conjugates from parkin. *EMBO J.* **33**, 2473–2491. (doi:10.15252/embj.201489729)
45. Ordureau A *et al.* 2018 Dynamics of PARKIN-dependent mitochondrial ubiquitylation in induced neurons and model systems revealed by digital snapshot proteomics. *Mol. Cell* **70**, 211–227. (doi:10.1016/j.molcel.2018.03.012)
46. McLelland GL *et al.* 2018 Mfn2 ubiquitination by PINK1/parkin gates the p97-dependent release of ER from mitochondria to drive mitophagy. *eLife* **7**, e32866. (doi:10.7554/eLife.32866)
47. Rakovic A, Shurkewitsch K, Seibler P, Grunewald A, Zanon A, Hagenah J, Krainc D, Klein C. 2013 Phosphatase and tensin homolog (PTEN)-induced putative kinase 1 (PINK1)-dependent ubiquitination of endogenous Parkin attenuates mitophagy: study in human primary fibroblasts and induced pluripotent stem cell-derived neurons. *J. Biol. Chem.* **288**, 2223–2237. (doi:10.1074/jbc.M112.391680)
48. Joaquim M, Escobar-Henriques M. 2020 Role of mitofusins and mitophagy in life or death decisions. *Front. Cell Dev. Biol.* **8**, 1002. (doi:10.3389/fcell.2020.572182)
49. Chen Y, Dorn II GW. 2013 PINK1-phosphorylated mitofusin 2 is a Parkin receptor for culling damaged mitochondria. *Science* **340**, 471–475. (doi:10.1126/science.1231031)
50. Yi W, MacDougall EJ, Tang MY, Krahn AI, Gan-Or Z, Trempe JF, Fon EA. 2019 The landscape of Parkin variants reveals pathogenic mechanisms and therapeutic targets in Parkinson's disease. *Hum. Mol. Genet.* **28**, 2811–2825. (doi:10.1093/hmg/ddz080)
51. Roberts RF, Wade-Martins R, Alegre-Abarrategui J. 2015 Direct visualization of alpha-synuclein oligomers reveals previously undetected pathology in Parkinson's disease brain. *Brain* **138**, 1642–1657. (doi:10.1093/brain/awv040)
52. Okatsu K *et al.* 2012 PINK1 autophosphorylation upon membrane potential dissipation is essential for Parkin recruitment to damaged mitochondria. *Nat. Commun.* **3**, 1016. (doi:10.1038/ncomms2016)
53. de Brito OM, Scorrano L. 2008 Mitofusin 2 tethers endoplasmic reticulum to mitochondria. *Nature* **456**, 605–610. (doi:10.1038/nature07534)
54. Smit JJ, Monteferrario D, Noordermeer SM, van Dijk WJ, van der Reijden BA, Sixma TK. 2012 The E3 ligase HOIP specifies linear ubiquitin chain assembly through its RING-IBR-RING domain and the unique LDD extension. *EMBO J.* **31**, 3833–3844. (doi:10.1038/emboj.2012.217)
55. Lechtenberg BC, Rajput A, Sanishvili R, Dobaczewska MK, Ware CF, Mace PD, Riedl SJ. 2016 Structure of a HOIP/E2–ubiquitin complex reveals RBR E3 ligase mechanism and regulation. *Nature* **529**, 546–550. (doi:10.1038/nature16511)
56. Stieglitz B, Morris-Davies AC, Koliopoulos MG, Christodoulou E, Rittinger K. 2012 LUBAC synthesizes linear ubiquitin chains via a thioester intermediate. *EMBO Rep.* **13**, 840–846. (doi:10.1038/embor.2012.105)
57. Kelsall IR, Zhang J, Knebel A, Arthur JSC, Cohen P. 2019 The E3 ligase HOIL-1 catalyses ester bond formation between ubiquitin and components of the Myddosome in mammalian cells. *Proc. Natl Acad. Sci. USA* **116**, 13 293–13 298. (doi:10.1073/pnas.1905873116)
58. Seenivasan R, Hermanns T, Blyszcz T, Lammers M, Praefcke GJK, Hofmann K. 2019 Mechanism and chain specificity of RNF216/TRIAD3, the ubiquitin ligase mutated in Gordon Holmes syndrome. *Hum. Mol. Genet.* **28**, 2862–2873. (doi:10.1093/hmg/ddz098)
59. Michel MA, Swatek KN, Hospenthal MK, Komander D. 2017 Ubiquitin linkage-specific affimers reveal insights into K6-linked ubiquitin signaling. *Mol. Cell* **68**, 233–246; e5. (doi:10.1016/j.molcel.2017.08.020)
60. Antico O *et al.* 2021 Global ubiquitylation analysis of mitochondria in primary neurons identifies endogenous Parkin targets following activation of PINK1. *Sci. Adv.* **7**, eabj0722. (doi:10.1126/sciadv.abj0722)
61. Watanabe M *et al.* 2020 A substrate-trapping strategy to find E3 ubiquitin ligase substrates identifies Parkin and TRIM28 targets. *Commun. Biol.* **3**, 592. (doi:10.1038/s42003-020-01328-y)
62. Escobar-Henriques M, Joaquim M. 2019 Mitofusins: disease gatekeepers and hubs in mitochondrial quality control by E3 ligases. *Front. Physiol.* **10**, 517. (doi:10.3389/fphys.2019.00517)
63. Basso V *et al.* 2018 Regulation of endoplasmic reticulum-mitochondria contacts by Parkin via Mfn2. *Pharmacol. Res.* **138**, 43–56. (doi:10.1016/j.phrs.2018.09.006)
64. Gelmetti V *et al.* 2017 PINK1 and BECN1 relocalize at mitochondria-associated membranes during mitophagy and promote ER-mitochondria tethering and autophagosome formation. *Autophagy* **13**, 654–669. (doi:10.1080/15548627.2016.1277309)
65. Rasool S, Veyron S, Soya N, Eldeeb MA, Lukacs GL, Fon EA, Trempe JF. 2022 Mechanism of PINK1 activation by autophosphorylation and insights into assembly on the TOM complex. *Mol. Cell* **82**, 1–16 (doi:10.1016/j.molcel.2021.11.012)
66. Gandhi S *et al.* 2009 PINK1-associated Parkinson's disease is caused by neuronal vulnerability to calcium-induced cell death. *Mol. Cell* **33**, 627–638. (doi:10.1016/j.molcel.2009.02.013)
67. Friedman JR, Lackner LL, West M, DiBenedetto JR, Nunnari J, Voeltz GK. 2011 ER tubules mark sites of mitochondrial division. *Science* **334**, 358–362. (doi:10.1126/science.1207385)
68. Kleele T *et al.* 2021 Distinct fission signatures predict mitochondrial degradation or biogenesis. *Nature* **593**, 435–439. (doi:10.1038/s41586-021-03510-6)
69. Vincow ES, Merrihew G, Thomas RE, Shulman NJ, Beyer RP, Maccoss MJ, Pallanck LJ. 2013 The PINK1-Parkin pathway promotes both mitophagy and selective respiratory chain turnover in vivo. *Proc. Natl Acad. Sci. USA* **110**, 6400–6405. (doi:10.1073/pnas.1221132110)
70. McWilliams TG, Prescott AR, Montava-Garriga L, Ball G, Singh F, Barini E, Muqit MMK, Brooks SP, Ganley IG. 2018 Basal mitophagy occurs independently of PINK1 in mouse tissues of high metabolic demand. *Cell Metab.* **27**, 439–449; e5. (doi:10.1016/j.cmet.2017.12.008)
71. Yang JY, Yang WY. 2013 Bit-by-bit autophagic removal of Parkin-labelled mitochondria. *Nat. Commun.* **4**, 2428. (doi:10.1038/ncomms3428)
72. Burman JL *et al.* 2017 Mitochondrial fission facilitates the selective mitophagy of protein aggregates. *J. Cell Biol.* **216**, 3231–3247. (doi:10.1083/jcb.201612106)
73. Di Rita A *et al.* 2018 HUWE1 E3 ligase promotes PINK1/PARKIN-independent mitophagy by regulating AMBRA1 activation via IKKalpha. *Nat. Commun.* **9**, 3755. (doi:10.1038/s41467-018-05722-3)
74. Yun J, Puri R, Yang H, Lizzio MA, Wu C, Sheng ZH, Guo M. 2014 MUL1 acts in parallel to the PINK1/Parkin pathway in regulating mitofusin and compensates for loss of PINK1/Parkin. *eLife* **3**, e01958. (doi:10.7554/eLife.01958)
75. Braschi E, Zunino R, McBride HM. 2009 MAPL is a new mitochondrial SUMO E3 ligase that regulates mitochondrial fission. *EMBO Rep.* **10**, 748–754. (doi:10.1038/embor.2009.86)
76. Yonashiro R *et al.* 2006 A novel mitochondrial ubiquitin ligase plays a critical role in mitochondrial dynamics. *EMBO J.* **25**, 3618–3626. (doi:10.1038/sj.emboj.7601249)
77. Nakamura N, Kimura Y, Tokuda M, Honda S, Hirose S. 2006 MARCH-V is a novel mitofusin 2- and Drp1-binding protein able to change mitochondrial morphology. *EMBO Rep.* **7**, 1019–1022. (doi:10.1038/sj.embor.7400790)
78. Koyano F, Yamano K, Kosako H, Tanaka K, Matsuda N. 2019 Parkin recruitment to impaired mitochondria for nonselective ubiquitylation is facilitated by MITOL. *J. Biol. Chem.* **294**, 10 300–10 314. (doi:10.1074/jbc.RA118.006302)
79. Ordureau A, Paulo JA, Zhang J, An H, Swatek KN, Cannon JR, Wan Q, Komander D, Harper JW. 2020 Global landscape and dynamics of Parkin and USP30-dependent ubiquitylomes in ineurons during mitophagic signaling. *Mol. Cell* **77**, 1124–1142; e10. (doi:10.1016/j.molcel.2019.11.013)
80. Phu L, Rose CM, Tea JS, Wall CE, Verschueren E, Cheung TK, Kirkpatrick DS, Bingol B. 2020 Dynamic regulation of mitochondrial import by the ubiquitin system. *Mol. Cell* **77**, 1107–1123; e10. (doi:10.1016/j.molcel.2020.02.012)

81. Sugiura A *et al.* 2013 MITOL regulates endoplasmic reticulum-mitochondria contacts via mitofusin2. *Mol. Cell* **51**, 20–34. (doi:10.1016/j.molcel.2013.04.023)
82. Fu M, St-Pierre P, Shankar J, Wang PT, Joshi B, Nabi IR. 2013 Regulation of mitophagy by the Gp78 E3 ubiquitin ligase. *Mol. Biol. Cell* **24**, 1153–1162. (doi:10.1091/mbc.e12-08-0607)
83. Schindelin J *et al.* 2012 Fiji: an open-source platform for biological-image analysis. *Nat. Methods* **9**, 676–682. (doi:10.1038/nmeth.2019)
84. Nielsen ML, Vermeulen M, Bonaldi T, Cox J, Moroder L, Mann M. 2008 Iodoacetamide-induced artifact mimics ubiquitination in mass spectrometry. *Nat. Methods* **5**, 459–460. (doi:10.1038/nmeth0608-459)